that students need to learn. The following explanation of the scientific report serves as a generic assignment for the sciences.

The Formal Scientific Research Report

A formal scientific research report is a piece of professional writing addressed to other professionals who are interested in the investigation you conducted. They will want to know why you did the investigation, how you did it, what you found out, and whether your findings were significant and useful. Research reports usually follow a standard five-part format: (1) introduction, (2) methods, (3) results, (4) discussion of results, and (5) conclusions and recommendations.

Introduction. Here you explain briefly the purpose of your investigation. What problem did you address? Why did you address it? You will need to provide enough background to enable the reader to understand the problem being investigated. Sometimes the introduction also includes a "literature review" summarizing previous research addressing the same or a related problem. In many scientific disciplines, it is also conventional to present a hypothesis—a tentative "answer" to the question that your investigation will confirm or disconfirm.

Methods. This is a "cookbook" section detailing how you did your investigation. It provides enough details so that other researchers could replicate your investigation. Usually, this section includes the following subsections: (a) research design, (b) apparatus and materials, and (c) procedures followed.

Results. This section, sometimes headed "Findings," presents the empirical results of your investigation. Often, your findings are displayed in figures, tables, graphs, or charts that are referenced in the text. Even though the data are displayed in visuals, the text itself should also describe the most significant data. (Imagine that the figures are displayed on a view graph and that you are explaining them orally, using a pointer. Your written text should transcribe what you would say orally.) Your figures and tables must have sufficient information to stand alone, including accurate titles and clear labels for all meaning-carrying features.

Discussion of results. This is the main part of the report, the part that will be read with the most care by other professionals. Here you explain the significance of your findings by relating what you discovered to the problem you set out to investigate in your introduction. Did your investigation accomplish your purpose? Did it answer your questions? Did it confirm or disconfirm your hypothesis? Are your results useful? Why or why not? Did you discover information that you hadn't anticipated? Was your research design appropriate? Did your investigation raise new questions? Are there implications from your results that need to be explored? The key to success in this section is to link your findings to the questions and problems raised in the introduction.

Conclusions and recommendations. In this last section, you focus on the main things you learned from the investigation and, in some cases, on the practical applications of your investigation. If your investigation was a pure research project, this section can be a summary of your most important findings along with recommendations for further research. If your investigation was aimed at making a practical decision (for example, an engineering design decision), here you recommend appropriate actions. What you say in this section depends on the context of your investigation and the expectations of your readers.

Redox Titration of Ferricyanide to Ferrocyanide with Ascorbic Acid: Illustrating the Nernst Equation and Beer–Lambert Law ⓦ

Tina H. Huang,* Gail Salter, Sarah L. Kahn, and Yvonne M. Gindt
Department of Chemistry, Lafayette College, Easton, PA 18042; *huangt@lafayette.edu

Electrochemistry and the Nernst equation are introduced in the chemistry curriculum at this college during second semester of general chemistry. The electrochemical concepts and applications are discussed further in analytical chemistry, physical chemistry, and biochemistry courses. Considering the prevalence of electrochemical concepts in many areas of chemistry, we feel that it is important that the students understand the fundamental electrochemical concepts early in the chemistry curriculum through hands-on experimentation. In the past, we had problems integrating an experiment that explained the Nernst equation well. For the last two years, we have incorporated a redox titration of ferricyanide ion, $[Fe(CN)_6]^{3-}$, to ferrocyanide ion, $[Fe(CN)_6]^{4-}$, to show the students how the reduction potential of a redox couple is affected by the concentrations of the redox species, and how they can use the Nernst equation to calculate the standard reduction potential of a half-reaction. While others have reported laboratory experiments dealing with the Nernst equation in this *Journal (1–4)*, these are usually written for more advanced courses such as physical chemistry and instrumental analysis and require techniques (i.e., cyclic voltammetry) that are often beyond the knowledge of typical first-year undergraduate students. In the experiment described here, our students obtain excellent data and we have encountered few problems with this laboratory.

The reduction of ferricyanide ion [or hexacyanoferrate(III)] to ferrocyanide [hexacyanoferrate(II)] coupled with the oxidation of ascorbic acid ($C_6H_8O_6$) to dehydroascorbic acid ($C_6H_6O_6$) was studied by Mehrotra, Agrawal, and Mushran *(5)*:

$$\underset{\text{(yellow)}}{\text{ferricyanide}} + e^- \longrightarrow \underset{\text{(colorless)}}{\text{ferrocyanide}} \quad (1)$$

$$\underset{\text{(colorless)}}{\text{ascorbic acid}} \longrightarrow \underset{\text{(colorless)}}{\text{dehydroascorbic acid}} + 2H^+ + 2e^- \quad (2)$$

We chose the ferricyanide/ferrocyanide redox system for this experiment because it is well-characterized *(5–9)*, and the concentration of ferricyanide can be easily monitored using UV–vis spectroscopy. We tried several other redox couples, but we found this system to be superior owing to its rapid equilibration time along with its relative inertness towards atmospheric oxygen.

In our general chemistry curriculum, the students are introduced to the concepts of electrochemistry and cell potential using the Nernst equation. While the students will be familiar with the expression given for the overall reaction, the expression using only the reduction of a species will be a new concept that must be introduced in the laboratory. For example, a generic reduction half-reaction, eq 3, and its corresponding Nernst expression, eq 4, are

$$A + ne^- \longrightarrow B \quad (3)$$

$$E = E^\circ - \frac{RT}{nF}\ln\frac{[B]}{[A]} \quad (4)$$

In eq 3, A is being reduced to B with the addition of n electrons. E° is the standard reduction potential of the A/B couple (one parameter that the students will find), while E is the reduction potential that the students monitor during the course of the titration for the specific conditions of [B] and [A]. The students will also find n, the number of electrons transferred during the reduction.

For the reduction of ferricyanide to ferrocyanide, we can write the Nernst expression as

$$E = E^\circ - \frac{RT}{nF}\ln\frac{[\text{ferro}]}{[\text{ferri}]} \quad (5)$$

where ferro and ferri are abbreviated forms of ferrocyanide and ferricyanide, respectively. Starting with only ferricyanide present in solution, small aliquots of ascorbic acid are added to the solution. After each aliquot, both the concentration of ferricyanide and the solution potential, E, are measured using UV–vis spectroscopy and a two-electrode potentiometric setup, respectively. The plot of the solution potential versus ln([ferro]/[ferri]) gives a line whose y intercept is the standard reduction potential of the ferrocyanide/ferricyanide couple. The number of electrons involved in the reduction of the couple, n, is easily calculated from the slope of the line. The ascorbic acid is used solely as the reductant in the reaction; we do not find the reduction potential of the ascorbic acid/dehydroascorbic acid couple.

The experiment provides an excellent illustration of the relationship between the concentration of species in a redox couple and the potential of the species. The students are exposed to a practical method of measuring a redox couple potential using spectroelectrochemistry.

Experimental Section

Reagents

Potassium hexacyanoferrate, $K_3Fe(CN)_6$, ascorbic acid, and potassium dihydrogen phosphate are purchased from Sigma-Aldrich (St. Louis, MO). All solutions are prepared using deionized water.

Instrumentation

The electrical potential, E, of the solution is monitored using a simple apparatus that had a platinum wire as working electrode, a saturated silver–silver chloride (Ag/AgCl) electrode as the reference electrode, and a digital voltmeter to monitor the difference in potential between the two electrodes. We also used either a Beckman Spec-20 (Sequoia Turner model 340) or an Ocean Optics (Chem 2000) UV–vis spectrophotometer to monitor the absorbance of the ferricyanide species in the solution.

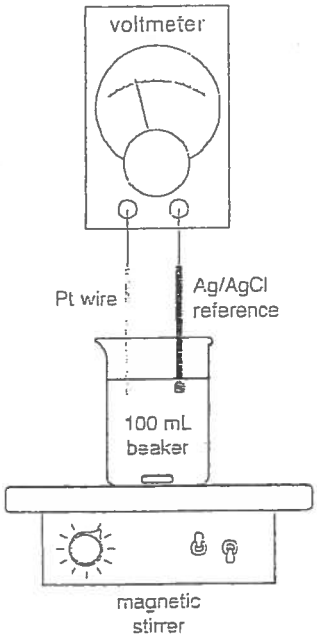

Figure 1. Experimental setup required for redox titration. The apparatus consists of a single Pt wire as the working electrode, a Ag/AgCl electrode as the reference electrode, and a voltmeter to monitor the potential of the Pt wire relative to the Ag/AgCl reference electrode.

Experimental Procedure

Two stock solutions, 0.50 mM $K_3Fe(CN)_6$ solution in 0.10 M pH 7 phosphate buffer and a 0.060 M ascorbic acid, are prepared by the instructor prior to the experiment. Approximately 30 mL of the ferricyanide solution and 1 mL of ascorbic solution are required by each group of students. The students start by immersing their platinum working electrode and the Ag/AgCl reference electrode in approximately 30 mL of 0.500 mM $K_3Fe(CN)_6$ solution (Figure 1). The solution is stirred constantly via magnetic stirring with special care taken to ensure the stir bar does not hit either electrode. Once the electrodes are set up properly and a stable voltage reading is obtained, a small portion of the bright yellow solution is removed to measure the absorbance of the ferricyanide at 420 nm. The solution is transferred back to the beaker after a successful absorbance reading. This absorbance is used to calculate the initial concentration of ferricyanide.

The students are now ready to begin their titration. A small aliquot, 5 μL, of 0.060 M ascorbic acid is added to the beaker with the electrodes. We generally use micropipets for the titration; it is critical to use small volumes of the titrant since we are making the approximation that the total volume of the solution is unchanged over the course of the experiment. We found that a 5 μL aliquot of titrant is optimal for the concentrations of solutions used; the students generally measure 15–20 samples over the course of the titration. Smaller volumes increase the length of the experiment while larger volumes decrease the number of data points used in the analysis.

After the ascorbic acid is added, the solution is allowed to equilibrate for two minutes. After two minutes, the potential and the absorbance at 420 nm are obtained; both readings should decrease over the course of the titration. Another aliquot of titrant is added at this point, and the entire process is repeated until the solution appears to be colorless.

Data Analysis

Our students analyze their data using the Excel spreadsheet. The calculations could also be done via a calculator. Using the Beer–Lambert law,

$$A = \varepsilon b c \tag{6}$$

the concentration, c, of ferricyanide is calculated from the absorbance of the solution. The molar absorptivity, ε, of the ion is 1.02×10^3 L mol^{-1} cm^{-1} and the path length, b, of 1 cm is used. The quantity of ferrocyanide is found from the quantity of ferricyanide lost during the titration, assuming no side reactions occur

$$[\text{ferri}]_{\text{initial}} = [\text{ferro}]_x + [\text{ferri}]_x \tag{7}$$

Table 1. Experimental Data Collected by One Group of Students

A	[ferri]/ (10^{-4} mol L^{-1})	[ferro]/ (10^{-4} mol L^{-1})	[ferro]/[ferri]	ln([ferro]/[ferri])	Potential/ mV
0.588	5.76	—	—	—	—
0.564	5.53	0.24	0.0433	-3.14	308.8
0.539	5.28	0.47	0.0890	-2.42	289.7
0.515	5.05	0.71	0.141	-1.96	277.9
0.493	4.83	0.93	0.193	-1.65	269.1
0.473	4.64	1.12	0.241	-1.42	261.6
0.445	4.36	1.40	0.321	-1.14	255.2
0.397	3.89	1.87	0.481	-0.732	244.7
0.373	3.66	2.10	0.574	-0.555	239.8
0.342	3.35	2.41	0.719	-0.330	233.6
0.297	2.91	2.85	0.979	-0.0212	225.6
0.273	2.68	3.08	1.15	0.140	221.2
0.248	2.43	3.33	1.37	0.315	216.7
0.211	2.07	3.69	1.78	0.577	209.9
0.162	1.59	4.17	2.62	0.963	200
0.143	1.40	4.36	3.11	1.13	195.6

where the subscript x indicates the [ferro] and [ferri] after the subsequent addition of ascorbic acid during the titration. The ln([ferro]/[ferri]) is calculated for each data point. To reduce problems owing to poor signal-to-noise at low concentrations of either species, data points outside the range of -1 to +1 for the ln([ferro]/[ferri]) are discarded from further analysis. The solution potential, E, is plotted versus ln([ferro]/[ferri]). The data are fit to a line using least-squares analysis. The y intercept is $E°$, the standard reduction potential of the ferrocyanide/ferricyanide couple versus the Ag/AgCl standard, and the negative slope of the line is RT/nF. Our students are able to solve the slope for n, given the constants and the temperature.

Hazards

There are no significant hazards associated with this experiment. The $[Fe(CN)_6]^{4-}$ and $[Fe(CN)_6]^{3-}$ are stable complex ions under the conditions of the experiment. The material data safety sheets for the complex ions do recommend the avoidance of strong acids and high temperature, which could cause the complex ion to decompose with the formation of hydrogen cyanide, a toxic gas. Also, both complex ions are toxic via ingestion.

Results

Typical data recorded during the course of the experiment for one group of students are shown in Table 1, while the data plotted as described above are shown in Figure 2. The average intercept value with the standard deviation is 0.228 ± 0.012 V and 0.224 ± 0.006 V for two different semesters. The standard reduction potential can be converted to the SHE standard by adding 0.197 V to the potential obtained with the Ag/AgCl standard (the value for the saturated Ag/AgCl electrode). The standard reduction potentials at pH 7 calculated by the students over the last two semesters (0.425 V and 0.421 V) agree well with the reported value of 0.430 V *(10)*. The number of electrons, n, calculated for the two different semesters are 1.04 ± 0.24 and 0.97 ± 0.05, respectively.

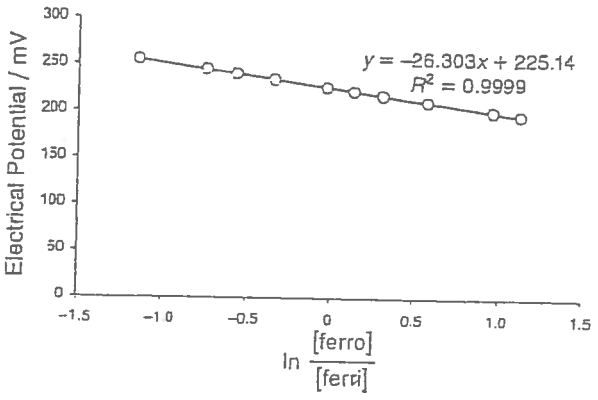

Figure 2. A plot of potential vs ln([ferro]/[ferri]) using the data in Table 1 (using potential range of 255.2–195.6 mV). The linear regression line is calculated using the trendline function in Microsoft Excel.

Conclusions

The redox titration of ferricyanide to ferrocyanide using ascorbic acid as the titrant is an effective method to illustrate the Nernst equation. The students can visually see the effect of the concentration term [ferro]/[ferri] in the Nernst equation on the potential measured. This laboratory also offers several additional benefits: The students use more advanced instrumentation and specialized equipment (i.e., reference electrodes, micropipetters) at the beginning of their chemistry curriculum. Also, they learn the process of using experimental data to calculate the standard reduction potential and number of electrons for the reduction half-reaction of ferricyanide to ferrocyanide. The laboratory forces the student to graphically interpret the Nernst equation.

A student survey was done at the end of the experiment: 80% of the students surveyed said they learned something new in the lab, and 82% said they would recommend that this lab be used in the future. Also, we have found the laboratory to have good reproducibility with outstanding results. It provides an excellent illustration of the Nernst equation for the experimental laboratory.

Acknowledgments

The authors wish to acknowledge Michael Chejlava for his technical assistance. This work was supported by the Department of Chemistry at Lafayette College.

Supplemental Material

Instructions for the students including a report form and notes for the instructor are available in this issue of *JCE Online*.

Literature Cited

1. Walczak, M. M.; Dryer, D. A.; Jacobson, D. D.; Foss, M. G.; Flynn, N. T. *J. Chem. Educ.* 1997, *74*, 1195–1197.
2. DeAngelis, T. P.; Heineman, W. R. *J. Chem. Educ.* 1976, *53*, 594–597.
3. Arévalo, A.; Pastor, G. *J. Chem. Educ.* 1985, *62*, 882–884.
4. Thompson, M. L.; Kateley, L. J. *J. Chem. Educ.* 1999, *76*, 95–96.
5. Mehrotra, U. S.; Agrawal, M. C.; Mushran, S. *J. Phys. Chem.* 1969, *73*, 1996–1999.
6. Kolthoff, I. M.; Tomsicek W. J. *J. Phys. Chem.* 1935, *39*, 945–954.
7. Blaedel, W. J.; Engstrom, R. C. *Anal. Chem.* 1978, *50*, 476–479.
8. Watkins, K. W.; Olson, J. A. *J. Chem. Educ.* 1980, *57*, 157–158.
9. Zahl, A.; van Eldik, R.; Swaddle, T. W. *Inorg. Chem.* 2002, *41*, 757–764.
10. Dutton, P. L. *Methods in Enzymology* 1978, *7*, 411–435.

State	T_e	ω_e	$\omega_e x_e$	B_e	α_e	D_e (10^{-4} cm^{-1})	r_e (Å)	Observed Transitions: Design.	Observed Transitions: ν_{00}	References
$^1H^{35}Cl$		μ = 0.97959272		$D_0^0 = 4.433_6$ eV[a]		I.P. = 12.74_8 eV[b]				DEC 1976 A
		Rydberg series corresponding to excitation of a 2p electron.						200-210 eV		(50)(60)
		Numerous absorption bands above 123000 cm^{-1}, tentatively assigned to higher members of the Rydberg series starting with L and M and converging to A $^2\Sigma^+$ of HCl^+.								(55)
M ($^1\Sigma^+$) (117811)		[1529]	v=0...5 observed. Assigned as $3p\sigma\,3p\pi^4\,5s\sigma$.[c]					M← X,	117093	(55)*
L ($^1\Sigma^+$,$^1\Pi$) 111280		1531	52	Assigned as $3p\sigma\,3p\pi^4\,4p\sigma/\pi$.[c]				L← X,	110555	(55)*
		Many other absorption bands in the region 83000 - 93000 cm^{-1} corresponding to Rydberg states strongly perturbed by the V $^1\Sigma^+$ state which itself gives rise to many perturbed bands.								(62)
K $^1\Pi$ (89861)		[2604.6]	z	[9.230][d]		[-12.6][d]	[1.3654]	K← X,	R 89680.5 z	(62)
H $^1\Sigma^+$ (89120)		[2093.8]	z	[8.4410]		[8.93]	[1.4278]	H← X,	R 88684.5 z	(62)
E $^1\Sigma^+$ (84193)		[2138.6]	z	[6.6423]		[36.2]	[1.6096]	E← X,	R 83780.2 z	(62)
g ($^3\Sigma^-$)1	e [84329.7]			[10.36][f]		[17][f]	[1.28_9]	g← X,	82847.4 z	(48)*
f_1 $^3\Delta_1$	e [84006.1]			[10.27_0][g]		[-13][g]	[1.294]	f_1← X,	82523.8 z	(48)*
D $^1\Pi$	h [83972.0]			[9.79_4][i]		[$20._5$][i]	[1.326]	D← X,	R 82489.7 z	(48)*
d_0 $^3\Pi_0$	h [83753.6]			[9.40_4][j]		[$-2._2$][j]	[1.353]	d_0← X,	R 82271.3 z	(48)*
f_2 $^3\Delta_2$	e [83497.7]			[10.85_1][k]		[$29._5$][k]	[1.259]	f_2← X,	V 82015.4 z	(48)*
f_3 $^3\Delta_3$	e [83308.2]			[9.45][g]		[$-1._3$][g]	[1.34_9]	f_3← X,	R 81825.9 z	(48)*
d_1 $^3\Pi_1$	h [83255.6]			[9.76_8][l]		[8][l]	[1.327]	d_1← X,	R 81773.3 z	(48)*
d_2 $^3\Pi_2$	h [83083.0]			[8.63_2][m]		[-14][m]	[1.412]	d_2← X,	R 81600.7 z	(48)*
C $^1\Pi$	n 77575	[2684.0]	z o	[9.33_3]	o		[1.358]	C← X,[p]	R 77485.3 z	(1)* (44)
V $^1\Sigma^+$	q $77293._0$	877.16	z 16.04[r]	2.727	-0.026	1.02[r]	2.512	V←→X,[s] V→A	R 76245.3 z	(8)(9)(48)* (9)
		Continuous emission spectrum with maximum at 38900 cm^{-1}.								

State	T_e	ω_e	$\omega_e x_e$	B_e	α_e	D_e (10^{-4} cm^{-1})	r_e (Å)	Observed Transitions: Design.	Observed Transitions: ν_{00}	References
$^1H^{35}Cl$ (continued)										
X $^1\Sigma^+$	0	2990.946_3[x]	52.8186[y]	10.59341_6[xz]	0.30718_1[a']	5.3194[zb']	1.27455_2[c']	Rot.-vibr. bands[d'e']		(19)(28)
								Rotation spectrum[f'e']		(4)(23)(52)
								Raman cross sections		(58)
								Mol. beam electric[g'] and magnetic[h'] reson.		(41)(64) (37)

$^1H^{35}Cl$ (continued):

[x] Applying the Dunham corrections (28) obtain $\omega_e = 2991.0904$ and $B_e = 10.593553$. Additional corrections (adiabatic, non-adiabatic) discussed by (49). Vibrational levels up to v=5 have been observed in infrared absorption (12)(19)(28) and emission (10), higher levels in the V→X bands (8)(9). Dunham potential coefficients (61). Most recent ab initio values of the ground state molecular constants (59); charge distribution (40).

[y] $\omega_e y_e = +\ 0.2243_7$, $\omega_e z_e = -\ 0.0121_8$ (28).

[z] Slightly different constants in (11)(26)(31). These papers and (39) give also constants for $H^{37}Cl$.

[a'] $+\ 0.001772_4(v+\frac{1}{2})^2 - 0.0001201(v+\frac{1}{2})^3$.

[b'] $-\ 7.51_0 \times 10^{-6}(v+\frac{1}{2}) + 4.0_0 \times 10^{-7}(v+\frac{1}{2})^2$; higher order terms in (28). See also (30).

[c'] Uncorrected value from the $B_e (\equiv Y_{01})$ given in the table. The internuclear distance at the minimum of the Born-Oppenheimer curve is $r_e = 1.2746149$ Å (49)(63).

[d'] Absolute intensities ($cm^{-2}atm^{-1}$) of the

1-0 band:	130	(5)
2-0 band:	2.9	(5)
	3.70	(17)(45)
3-0 band:	0.023	(5)

[e'] Pressure-induced shifts (by foreign gases) of rotation-vibration and rotation lines (13)(14)(21)(22)(24). For discussions of pressure-induced bands and pure rotation lines (ΔJ=2) see (32)(36). Self and foreign-gas line broadening (5)(7)(16)(17)(18)(29)(43)(45)(47)(52). Infrared absorption in liquid and solid phases (42)(51).

[f'] Absolute intensity measurements (25)(34).

[g'] $\mu_{e\ell}(v=0,1,2) = 1.1085$, 1.1390, 1.1685 D, resp. (41). Dipole moment function (41)(54); see also (53)(56). $g_J = 0.4594$, also quadrupole and other hyperfine coupling constants (41)(64); see also (35)(53).

[h'] Proton spin - rotation interaction constant (15)(37).

State	T_e	ω_e	$\omega_e x_e$	B_e	α_e	D_e (10^{-4} cm^{-1})	r_e (Å)	Observed Transitions: Design.	Observed Transitions: ν_{00}	References
$^2H^{35}Cl$		μ = 1.90441364		$D_0^0 = 4.485_2$ eV[a]		I.P. = 12.75_6 eV[b]				DEC 1976 A
		Numerous absorption bands above 123000 cm^{-1}; see ^{1}HCl.								(25)
M ($^1\Sigma^+$) (117670)		[1220] v=0...8 observed.						M ← X,	117214	(25)
L ($^1\Sigma^+$, $^1\Pi$) 111268		1126 37 } See ^{1}HCl.						L ← X,	110748	(25)
		Many other absorption bands in the region 83000 - 93000 cm^{-1}; see ^{1}HCl.								(27)
K $^1\Pi$	(89945)	[1858.8] z		[4.9306][c]			[1.3399]	K ← X, R	89708.9 z	(27)
H $^1\Sigma^+$	(88944)	[1631.8] z		[4.6578]		[0.14$_7$]	[1.3786]	H ← X, R	88694.0 z	(27)
E $^1\Sigma^+$	(84417)	[1186.9] z		[3.2960]		[-2.48]	[1.6388]	E ← X, R	83944.9 z	(27)
f_1 $^3\Delta_1$	[83626.2]			[5.21$_0$]		[0.96]	[1.303]	f_1 ← X, R	82560.4 z	(22)
D $^1\Pi$	(82632)	[1918.8] z		5.14$_2$[d]	0.152	[2.$_0$][d]	1.312	D ← X, R	82525.9 z	(22)
d_0 $^3\Pi_0$	[83350.3]			[5.01$_6$]		[1.3$_5$]	[1.328]	d_0 ← X, R	82284.5 z	(22)
f_2 $^3\Delta_2$	[83140.0]			[5.32$_8$]		[3.9]	[1.289]	f_2 ← X, R	82074.2 z	(22)
d_1 $^3\Pi_1$	[82855.0]			[5.13$_7$][e]		[1.9][e]	[1.313]	d_1 ← X, R	81789.2 z	(22)
d_2 $^3\Pi_2$	[82695.6]			[4.74$_7$][f]		[-7][f]	[1.366]	d_2 ← X, R	81629.8 z	(22)
C $^1\Pi$	77558.5	2027.1 z	34.98[g]	4.962[h]	0.120	[1.16]	1.336	C ← X, R	77497.6 z	(9)(18)*
b_0 $^3\Pi_0$	[76548.0]			[5.21$_8$]			[1.302]	b_0 ← X, R	75482.2 z	(18)*
b_1 $^3\Pi_1$	75199.3	2015.4 z	29.1	[5.10$_0$][i]	0.12$_9$[j]	[3.$_5$]	1.309	b_1 ← X, R	75133.9 z	(9)(18)*
b_2 $^3\Pi_2$	[75912.7]			[4.90$_5$]			[1.343]	b_2 ← X, R	74846.9 z	(18)*
X $^1\Sigma^+$	0	2145.163 z	27.1825[k]	5.448794[l]	0.113291[k]	1.39[m]	1.274581	Rot.-vibr. bands[nop]		(2)(3)(7)(8)
								Rotation sp.[p]		(1)(5)(21)(23)
								Mol. beam el. reson.[q]		(16)

2090.80 = 2145.163 − 2(27.1825)

Vibrations of Carbon Dioxide and Carbon Disulfide

Purpose

Vibration frequencies of CO_2 and CS_2 will be measured by Raman and Infrared spectroscopy. The spectra show effects of normal mode symmetries on gross selection rules. A Fermi resonance in the Raman spectrum will be interpreted in terms of interacting normal modes. Vibration frequencies will be calculated with *ab initio* quantum-chemical methods and compared to experimental frequencies. CS_2 has longer bonds and lower vibration frequencies than CO_2.

Introduction

Linear triatomic molecules such as CO_2 and CS_2 have four vibrational normal modes but just three fundamental vibration frequencies because two modes are degenerate.[1] The stretching mode is totally symmetric so it is inactive in infrared spectra and active in Raman spectra. The

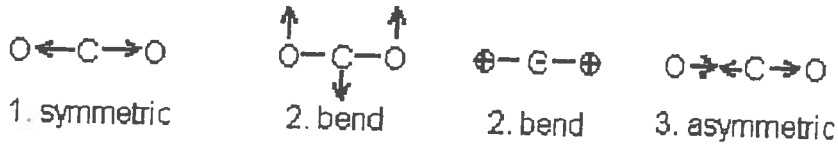

asymmetric stretching vibration and the degenerate bending vibrations are infrared active and Raman inactive. Infrared activities follow from the gross selection rule that "displacements of a normal mode must cause a change in dipole moment in order to be spectroscopically active in the infrared."[1] The CO_2 and CS_2 molecules have a center of symmetry located at the carbon atom. Such molecules obey the exclusion rule, "In a centrosymmetric molecule no Raman-active molecule is also infrared-active and no infrared-active vibration is also Raman active."[2] The symmetric stretching vibration is Raman active and infrared inactive. The bend and asymmetric stretch are infrared active and are, for CO_2, routinely observed in the background scan on an FTIR instrument.[3]

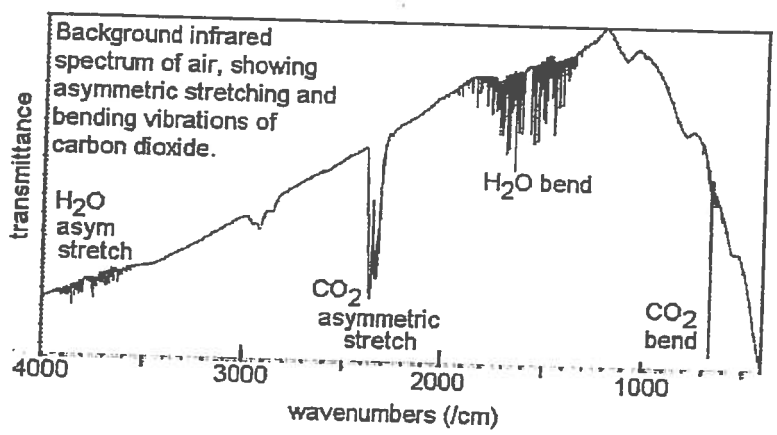

Vibration frequencies will be calculated quantum-mechanically for both CO_2 and CS_2, using three methods: Hartree Fock, Hartree Fock plus second-order Moller-Plesset correction, and density functional theory. Hartree-Fock calculations are the simplest and most robust of the three methods and are good for initial geometry optimization. Vibration frequencies calculated from simple Hartree Fock theory are usually too large by about 10%. Second-order Moller-Plesset

2349

3 2

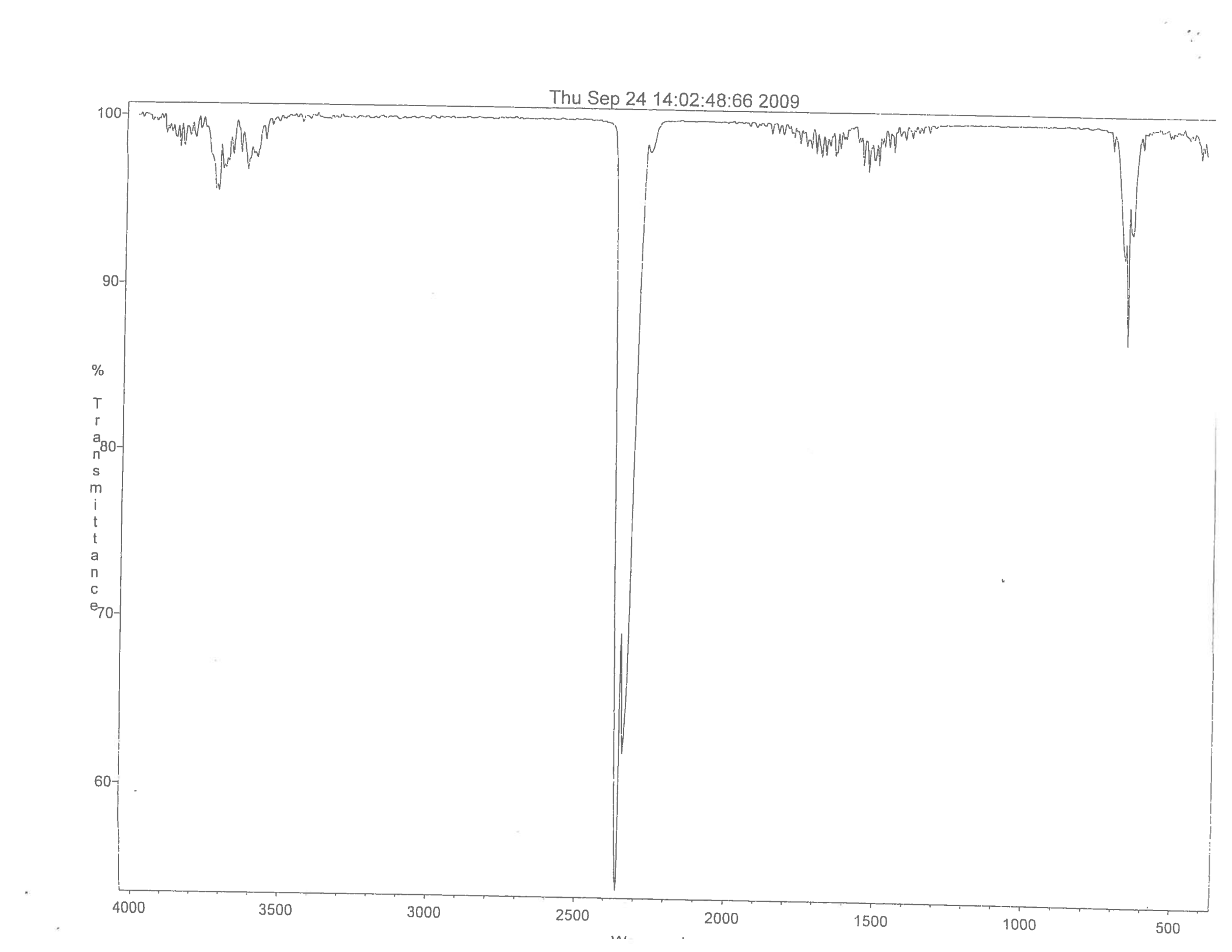
Thu Sep 24 14:02:48:66 2009
100
90
80
70
60
% Transmittance
4000
3500
3000
2500
2000
1500
1000
500

TABLE 64 (*continued*)

State	Point Group	T_0	Vibrational Frequencies ν_1	ν_2	ν_3	Rotational Constants A_0	B_0	C_0	r_0(XY)	r_0(YZ)	α	Electron Configuration	Observed Transitions	References	Remarks
	CO_2	I.P. = 13.769 eV; D(O—CO) = 5.453 eV (see energy level diagram Fig. 19b)													
		Three broad continua with maxima at 570, 350 and 280 Å												(80)	
		Three Rydberg series: $\nu = 156390 - \begin{cases} R/(n+0.29)^2; & n=3,\ldots,8 \\ R/(n+0.44)^2; & n=3,\ldots,8 \\ R/(n-0.05)^2; & n=4,\ldots,8 \end{cases}$ with first members at 146490, 147280 and 149500 respectively, converging to a new state of CO_2^+ viz. the predicted $^2\Sigma_g^+$												(1189)	
		Two Rydberg series joining on to $\bar{R}$ and $\bar{S}$: $\nu = 145800 - \begin{cases} R/(n+0.008+3.25/n^3)^2; & n=3,\ldots,18 \\ R/(n-0.305)^2; & n=3,\ldots,18 \end{cases}$ [a] converging to the $^2\Sigma_u^+$ state of CO_2^+												(1191)	Henning series; see Fig. 18b, p. 502
$\bar{S}$	$D_{\infty h}$	132977	1273										$\bar{S} \leftarrow \tilde{X}$ 752 Å	(1191)	Sharp bands; repr. (1191)
$\bar{R}$	$D_{\infty h}$	130774	1275										$\bar{R} \leftarrow \tilde{X}$ 765 Å	(1191)	Diffuse bands; repr. (1191)
		Rydberg series joining on to $\bar{L}$: $\nu = 139720 - R/(n - 0.063 - 0.0009/n)^2$; $n = 3,\ldots,10$,												(1191)	Converging to the $^2\Pi_{\frac{1}{2}u}$ state of CO_2^+ [b]
		Rydberg series parallel to above: $\nu = 139634 - R/(n - 0.044 - 0.34/n)^2$; $n = 4,\ldots,9$												(1191)	Converging to the $^2\Pi_{\frac{1}{2}u}$ state of CO_2^+ [b]
$\bar{M}$		127443	1120										$\bar{M} \leftarrow \tilde{X}$ 784–758 Å	(1191)	Progression of five members
$\bar{L}$	$D_{\infty h}$	127065	1127										$\bar{L} \leftarrow \tilde{X}$ 787–712 Å	(1189) (1191)	Progression of six members; repr. (1191)
		Two weak Rydberg series joining on to $\bar{E}$ and $\bar{G}$: $\nu = 111250 - \begin{cases} R/(n-0.57)^2; & n=3,4,\ldots,11 \\ R/(n-0.97)^2; & n=4,5,\ldots,11 \end{cases}$												(1189)	
		Two strong Rydberg series joining on to $\bar{D}$, $\bar{H}$ and $\bar{I}$: $\nu = \begin{cases} 111240 \\ 111060 \end{cases} - R/(n-0.65)^2$; $n = 3, 4, \ldots, 15$ [c]												(1189)	Converging to $^2\Pi_{\frac{1}{2}g}$ and $^2\Pi_{\frac{1}{2}g}$ of CO_2^+

CO_2:

[a] Each series is accompanied by a vibrational series separated from the main series by 1274 cm^{-1} which corresponds to $\Delta G_{\frac{1}{2}}$ in the $^2\Sigma_u^+$ state of CO_2^+.

[b] Each member consists of a long progression in ν_1 with spacings similar to those in $^2\Pi_u$ of CO_2.

[c] In addition a vibrational series, 1410–1260 cm^{-1} to shorter wavelengths, has been observed corresponding to the first ΔG in the ground state of CO_2^+.

TABLE 64 (*continued*)

State	Point Group	T_0	Vibrational Frequencies ν_1 ν_2 ν_3	Rotational Constants A_0 B_0 C_0 $r_0(XY)$ $r_0(YZ)$ α	Electron Configuration	Observed Transitions	References	Remarks
CO_2 (*continued*)								
I	$D_{\infty h}$	100040				$I \leftarrow \bar{X}$ 901 Å	(1189)	
$\bar{H}$	$D_{\infty h}$	{100650 100570				$\bar{H} \leftarrow \bar{X}$ 994 Å	(1189)	
$\bar{G}$		99331				$\bar{G} \leftarrow \bar{X}$ 1007 Å	(1189)	
$\bar{F}$	$(D_{\infty h})$	96000	1320			$\bar{F} \leftarrow \bar{X}$ 1035–960 Å	(1058)(1189)	
$\bar{E}$	$(D_{\infty h})$	{92360 91830	{1240 1172			$\bar{E} \leftarrow \bar{X}$ 1070–1010 Å	(1058)(1189)	A weak and a strong progression
$\bar{D}$	$D_{\infty h}$	{89111 88535	{1567 1458			$\bar{D} \leftarrow \bar{X}$ {1120–1122 Å	(1189)	Very strong, violet shaded bands
$\bar{C}$	$D_{\infty h}$	{85840 85160	{1165 1270			$\bar{C} \leftarrow \bar{X}$ 1170–1130Å	(1058)(1189)	A weak and a strong progression
$B\left\{{}^1B_1(\Sigma_g^-)\right.$ $\left.{}^1A_1(\Delta_g)\right\}$	(C_{2v})	{73100 72480	(1225)		{$\ldots b_1 a_1^2 a_2^2 b_2^2 a_1$ $\ldots b_1^2 a_1 a_2^2 b_2^2 a_1$	$\bar{B} \leftarrow \bar{X}$ 1390–1220 Å	(1021)(604)	Distinct red shaded bands, possibly two systems
$\bar{A}\,{}^1B_2(\Delta_u)$	C_{2v}	46000		5.3 $\bar{B}=0.420$ 1.246 122° ±2°	$\ldots 1\pi_u^4 a_2^2 b_2 a_1$	$\bar{A} \leftrightarrow \bar{X}$ [d]	(1021)(604) (283)	In absorption weak diffuse bands[e]
$\bar{X}\,{}^1\Sigma_g^+$	$D_{\infty h}$	0	1388.17[f][g] 667.40[f] 2349.16[f]	— 0.39021[h] — 1.1021 180°	$\ldots 4\sigma_g^2 3\sigma_u^2 1\pi_u^4 1\pi_g^4$	Raman and infrared sp.	(1160)(1085) (605)(245)	

CO_2: [d] In absorption 1750–1400 Å, in emission 3800–3100 Å. [e] Overlapped by continuum; in emission carbon monoxide flame bands; see (283).
[f] For the anharmonic constants x_{1k} see (246). [g] Shifted by Fermi resonance with $2\nu_2^0$ which is at 1285.40 cm^{-1}.
[h] $a_1 = 0.00121$, $a_2 = -0.00072$, $a_3 = 0.00309$; $D = 13.5 \times 10^{-8}$.

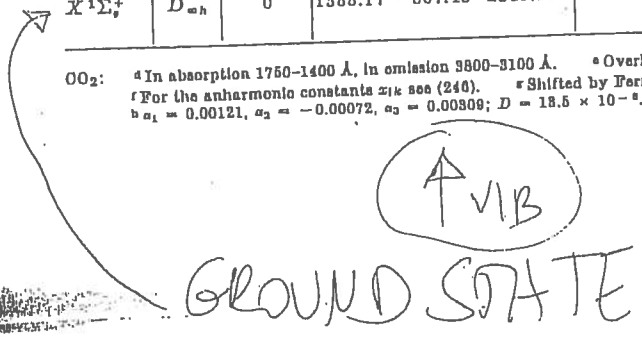

TABLE 64 (*continued*)

$D_0(O_2) \approx D_0(H_2O) = 5.$

(exp) 5.115eV

State	T_e	ω_e	$\omega_e x_e$	B_e	α_e	D_e (10^{-2} cm^{-1})	r_e (Å)	Observed Transitions: Design.	Observed Transitions: ν_{00}	References
$^1H_2$		$\mu = 0.50391261$		$D_0^0 = 4.4781_3$ eV[a] ≈ OH (4.34) ≈ HCl (4.43)						I.P. = 15.4258_9 eV[b]
		WAVELENGTH TABLES of the H_2 spectrum from 2800 to 29000 Å with assignments of many of the lines (109). The TABLES OF ENERGY LEVELS (24) are also very useful as long as it is realized that the absolute values of the energy levels ($n \geq 2$) relative to the ground state need correction. Graphs and tables of POTENTIAL ENERGY CURVES for all known states of H_2, H_2^+, and H_2^- (107).									NOV 1976 A
	See [v] p. 241	Fragments of three other triplet systems.[c]								
u $^3\Pi_u$ 6pπ [123488.$_0$]		Only v=0 observed.		[29.3]		[2.3]	[1.06$_9$]	u→a, δ bands	26232.3[f]	(1)(24)
t[d] $^3\Sigma_u^+$ 5fδ (121292)		(2661.4)	(121.9)	e				t→a,	(25342)	(4)
q[d] ($^3\Sigma_g^+$) 5dδ (121295)		[2172.6]		e				q→c,	(25325)[f]	(3)
n $^3\Pi_u$ 5pπ 120952.$_9$		2321.4	62.8$_6$	29.9$_5$	1.24[g]	[2.3]	1.057	n→a, γ bands	24847.3[f]	(1)(24)
m[h] $^3\Sigma_u^+$ 4fδ (119317)		[2457.1]		e				m→a,	23295.1[i]	(4)
s $^3\Delta_g$ 4dδ 118875.$_2$		2291.7[j]	62.4$_4$[j]	k				s→c,	22949.3[ℓ]	(1)(18)(24)
r $^3\Pi_g$ 4dπ 118613.$_7$		2280.3[m]	57.9$_6$[m]	k				r→c,	22683.2[m]	(1)(18)(24)
p $^3\Sigma_g^+$ 4dδ 118509.$_8$		2303.1	76.9$_0$	e				p−k,[n]		(154)
v ($^3\Pi_g$) [o] (118330)		(2340)	(57)	([29.1])			([1.07$_2$])	p→c,	22586.0[f]	(1)(18)(24)
k $^3\Pi_u$ 4pπ 118366.$_2$[p]		2344.37	67.2$_9$[q]	30.07$_4$	1.46$_2$[r]	[1.8$_5$]	1.054$_7$	v→c,	(22430)	(3)
f $^3\Sigma_u^+$ 4pδ (116705)		[2143.6][s]		[27.0][s]			[1.11]	k→a, β bands	22271.0[f]	(1)(15a)(24)
o[t] $^3\Sigma_u^+$ (114234)		2399.1	91.0	[35]			[0.98]	f→a,	20526.0[s]	(1)(24)
ℓ[u] $^3\Pi_u$ 113825		2596.8	106.0	[36]			[0.96]	o→a,	(18160)	(4)
								ℓ→a,	17846[f]	(4)

State	T_e	ω_e	$\omega_e x_e$	B_e	α_e	D_e (10^{-2} cm^{-1})	r_e (Å)	Observed Transitions: Design.	Observed Transitions: ν_{00}	References
$^1H_2$ (continued)										
B $^1\Sigma_u^+$ $2p\sigma$	91700.0[a]	1358.09	20.888[b]	20.015_4[c]	1.1845[d]	1.625[e]	1.2928_2	$B^f \leftrightarrow X$,[gh] Lyman b.	R 90203.3_5	(25)(77)(129)
X $^1\Sigma_g^+$ $1s\sigma^2$	0	4401.21_3	121.33_6[i]	60.853_0[k]	3.062_2[j]	4.71[l]	0.74144	Quadrupole[m] and field-induced sp..[n]		(15)(48) (26)(56)(74)
								Raman sp.[o]		(23)(56)
								Rotational[p] and nuclear rf magn. reson.		(17a)(21) (17)(19)

$^1H_2$: [a] See n p. 249.

[b] $+ 0.7196(v+\frac{1}{2})^3 - 0.0598(v+\frac{1}{2})^4 + 0.00216(v+\frac{1}{2})^5$, $Y_{00} = 8.7$; from a least squares fit (129) to the first eight levels as given by (25). (77) gives slightly different constants based on the first five levels only. (73) and (37) have observed levels up to v=35 and 37, resp., very close to the dissociation limit at 118377.6 cm^{-1} (95). The dissociation energy of the B $^1\Sigma_u^+$ state is 28174.2 cm^{-1}.

[c] RKR potential functions (31)(44)(72)(89); see also (126). Precise ab initio potential function (incl. diagonal corrections) and predicted vibrational levels (67)(152).

[d] $+ 0.1214(v+\frac{1}{2})^2 - 0.0117(v+\frac{1}{2})^3 + 0.0004_6(v+\frac{1}{2})^4$, from a least squares fit (129) to the first eight levels. (77) gives slightly different constants based on the first five levels only. For $v \geq 8$ there are strong rotational perturbations caused by interaction with C $^1\Pi_u$. Only after deperturbation can meaningful B_v values for these levels be obtained [see (129)]. For a theoretical discussion of the intensities in the perturbed region see (131).

[e] $- 2.16_5 \times 10^{-3}(v+\frac{1}{2}) + 2.28_9 \times 10^{-4}(v+\frac{1}{2})^2 - 1.18_5 \times 10^{-5}(v+\frac{1}{2})^3$. For individual B_v and D_v values see (25)(37)(129).

[f] Lifetime $\tau(v=3...7) = 0.8$ ns (66); $\tau(v=8...11) = 1.0$ ns (111).

[g] Franck-Condon factors from RKR potentials (51)(89); from ab initio potential functions (64)(90)(91), including theoretical oscillator strengths; see also (167). J dependence of Franck-Condon factors and transition probabilities (87)(88)(102). Experimental Franck-Condon factors and oscillator strengths (57)(65)(69)(83)(130)(142)(157); $\Sigma f_{v'0} = 0.29$. Variation of transition moment with r (69)(83)(157) and, ab initio, (64)(88). Selective enhancements of v=3 and 10 of B $^1\Sigma_u^+$ in an Ar-H_2 mixture, first observed by Lyman,

State	T_e	ω_e	$\omega_e x_e$	B_e	α_e	D_e ($10^- cm^{-1}$)	r_e (Å)	Observed Transitions: Design.	Observed Transitions: ν_{00}	References
$^{16}O_2$		$\mu = 7.9974575_1$		$D_0^0 = 5.115_6$ eV[a]		I.P.($1\pi_g$) = 12.071 eV[b] ($1\pi_u$) = 16.092 eV[c] ($3\sigma_g$) = 18.159 eV[c] ($2\sigma_u$) = 24.549 eV[c] ($2\sigma_g$) = 39.6 eV[d] ($1s_O$) = 543.1 eV[d]				MAR 1977 A
A detailed review of the entire spectrum of molecular oxygen has been published by (141).										
Potential energy diagrams (63)(128)(141)(190); predicted electronic states and potential functions (167)(176)(182).										
z ($^3\Pi_u$)		Several Rydberg states converging to the oxygen K limits at 543.1($^4\Sigma^-$) and 544.2($^2\Sigma^-$) eV, in X-ray absorption and electron energy loss spectra. Strong X-ray absorption peak (excitation $1s_O \rightarrow 1\pi_g$).						Z ← X,	532 eV[e]	(133)(166)(175)
Absorption cross sections and cross sections for the production of atomic fluorescence by photodissociation in the region 175 - 850 Å (570000 - 115000 cm^{-1}) (156)(158)(161)(164). Earlier results in (18)(23)(58).										
		Rydberg states with the outer electrons in 3sσ, 3pσ, 3dσ orbitals and the O_2^+ core in the highest $...1\pi_u^3\, 1\pi_g^2\, ^2\Pi_u$ state have been tentatively identified in the electroionization spectrum of O_2 at 20.73, 21.75, 22.28 eV, respectively.								(160)
		Codling and Madden's Rydberg series converging to c $^4\Sigma_u^-$(v=0) of O_2^+ ; $\nu = 198125 - \begin{cases} R/(n-0.16)^2 & n = 3\,(Y\text{ state}),4...11.^{fg} \\ R/(n-0.95)^2 & n = 3\,(W\text{ state}),4....8.^{fgh} \end{cases}$ Similar series with v'=1.								(65)*
Y ^{f} (184440)		[1510]		^{g}				Y ← X,	184410	(65)*
W ($^3\Sigma_u^-$)^f (168290)		[1510]		^{g}				W ← X,	168260	(65)*
		Yoshino and Tanaka's weak Rydberg series converging to B $^2\Sigma_g^-$(v=0) of O_2^+ ; $\nu = 163700 - R/(n-0.54)^2$ $n = 6\,(V\text{ state}),7...12.^f$ Similar series with v'=1,2,3.								(98)
V ^{f} (160270)		(1100)						V ← X,	160031	(98)
		Tanaka and Takamine's strong Rydberg s. of R shaded dif. b. converging to B $^2\Sigma_g^-$(v=0) of O_2^+ ; $\nu = 163702 - R/(n-0.70)^2$ $n = 3\,(U\text{ state}),4...23.^{fi}$ Similar series with v'=1,2,3.								(9)(86)*(98)*

State	T_e	ω_e	$\omega_e x_e$	B_e	α_e	D_e	r_e	Observed Transitions	References

State	T_e	ω_e	$\omega_e x_e$	B_e	α_e	D_e (10^{-6} cm^{-1})	r_e (Å)	Observed Transitions: Design.	Observed Transitions: ν_{00}	References
$^{16}O_2$ (continued)										
b $^1\Sigma_g^+$	13195.1	1432.77[a]	z 14.00[a]	1.40037[a]	0.01820[a]	5.351[b]	1.22688	b→a,[c]	5238.5	(40)
								b↔X,[de] R	13120.91[f] z	(12)*
								Atmospheric oxygen b.		
a $^1\Delta_g$	7918.1	[1483.5$_0$]	z (12.$_9$)	1.4264	0.0171	[4.86]	1.2156$_3$	a[g]↔X,[he] R	7882.39 z	(10)*
								IR atmosph. oxygen b.		
X $^3\Sigma_g^-$	0	1580.19$_3$	z 11.98$_1$[i]	[1.4376766][j] B_e = 1.44563	0.0159$_3$[kl]	[4.839][jl]	1.20752	Rot.-vibr. sp. (collision induced)		(12a)(75a) (142)
								Rotation sp.[mn]		(94)(105)
								Spin reorientation (fine structure) sp.[mo]		(20)(41)(76) (120)(159)
								Raman sp.[p]		(38)* (124)* (162)(183)*
								EPR sp.		(25)(138)(154)

O_2,

[a] These constants have been re-evaluated [(148), see also (168)] from the measurements of the b−X system (12) using improved lower state constants; $\gamma_e = -0.00004_2$. RKR potential curve (148). Constants for $^{16}O^{18}O$, $^{16}O^{17}O$ in (12).

[b] $+ 0.0318(v+\frac{1}{2}) + 0.0012(v+\frac{1}{2})^2$. The D_v values have been calculated (148) using vibrational wavefunctions computed from the experimental potential curve; see (147).

[c] Q branch of the 0-0 band observed in a discharge through O_2 and He. Absolute transition probability $\sim 2.5 \times 10^{-3}$ s^{-1}.

[d] In absorption observed in the solar spectrum; in the laboratory with more than 1 m path. In emission in the aurora and nightglow (14) as well as in various discharges (11) (15)(39)(40). Band intensities [in cm^{-1}km^{-1}atm^{-1}(STP)] for the 0-0, 1-0, 2-0 bands are 532, 40.8, 1.52, respectively (102); slightly smaller values in (137). The transition probability for the 0-0 band is 0.075 s^{-1} [average of values given by (102) and (137)]. (49) gives the band oscillator strengths $f_{00} = 2.5 \times 10^{-10}$, $f_{10} \approx 0.2 \times 10^{-10}$. RKR Franck-Condon factors (141)(190); rotational intensity distribution and pressure broadening (100)(102)(137).

[e] Pressure induced spectra a← X, b← X as well as simultaneous transitions in two colliding molecules have been studied by many investigators. See recent papers by (116)(142) which refer to earlier work.

[f] (148) give $\nu_{00} = 13122.235$ cm^{-1}, differing by $+\frac{2}{3}\lambda$ (spin-spin interaction in X $^3\Sigma_g^-$) from the zero line of (12).

State	T_e	ω_e	$\omega_e x_e$	B_e	α_e	D_e (10^{-} cm^{-1})	r_e (Å)	Observed Transitions: Design.	Observed Transitions: ν_{00}	References
$^{14}N_2$		μ = 7.00153720		D_0^0 = 9.759$_4$ eV[a]						FEB 1977 A
							I.P.($3\sigma_g$) = 15.5808 eV[b]			
							($1\pi_u$) = 16.6986 eV[bc]			
							($2\sigma_u$) = 18.7507 eV[b]			
							($2\sigma_g$) = 37.9 eV[d]			
							($1s_N$) = 409.9$_8$ eV[e]			

For a very detailed and critical review of the spectrum of molecular nitrogen and its ions see the recent publication by Lofthus and Krupenie (196). Atlas of the VUV absorption spectrum 1060 - 1520 Å and table of absorption lines (87). Tables of band head wavelengths (39)(48)(196). Photoionization and absorption cross sections (45)(57)(147). Potential functions (60)(68)(182)(196).

$x''(^1\Sigma_u^+)$		Several Rydberg series (excitation of $1s_N$) with limit (K edge) at 409.5 eV.						
$x'(^1\Pi_u)$		X-ray absorption ($3s\sigma \leftarrow 1s_N$).						
		X-ray absorption and emission ($1\pi_g \leftrightarrow 1s_N$), broad peak.[f]			$x'' \leftarrow X$,	405.5$_9$ eV		(114)(166) (173)(174)
					$x' \leftrightarrow X$,	400.8$_4$ eV		
		Photoionization and dissociative photoionization processes corresponding to various excited states of N_2^+.[g]						(177)(194)
v	$^1\Pi_g$	From high-energy electron impact spectroscopy.						
u_5	(183640)	Fragments of other progressions and unassigned bands, 198000 - 207000 cm^{-1}.			$v \leftarrow X$,	253000		(180)
u_4	(178565)	(2100) (15)						
		(2070) (15)	First two members of Codling's Rydberg series.[h]					
$\ldots 2\sigma_u\, 1\pi_u^4\, 3\sigma_g^2 \{ns\sigma$		Hopfield's Rydberg series converging to B $^2\Sigma_u^+(v=0)$ of N_2^+,			$u_5 \leftarrow X$,	(183510)		(76)(163)
$nd\sigma\}$		$\nu = 151233 - \begin{cases} R/(m + 0.141 - 0.199/m)^2, & m = 3\ldots11 \text{ (apparent emission series)}^{ijk\ell} \\ R/(m - 0.070 - 0.041/m)^2, & m = 3\ldots20 \text{ (absorption series)} \end{cases}$			$u_4 \leftarrow X$,	(178420)		
$\ldots 2\sigma_u^2\, 1\pi_u^3\, 3\sigma_g^2\, ns\sigma$		Worley's ("third") Rydberg series joining on to o_3, o_4, o_5 and converging to A $^2\Pi_{u\frac{1}{2}}(v=0)$ of N_2^+,						(1)(4)* (37)*
		$\nu = 134721 - R/(n - 1.06)^2$, $n = 3\ldots16$.[mnop]						
$\ldots 2\sigma_u^2\, 1\pi_u^3\, 3\sigma_g^2\, ns\sigma$	q	Ogawa and Tanaka's Rydberg series joining on to o_4, o_5 and converging to A $^2\Pi_{u\frac{3}{2}}(v=0)$ of N_2^+,						(8)(37)* (190)*
		$\nu = 134644 - R/n^{*2}$, $n^* = 2.84, 3.85, 4.86, \ldots, 14.91$.[mnop]						
		Several dissociation continua in the region 100000 - 160000 cm^{-1}.						(37)* (190)*
		Several unidentified bands in the region 126100 - 131550 cm^{-1}.						(105)(156) (51)

State	T_e	ω_e	$\omega_e x_e$	B_e	α_e	D_e	r_e	Observed Transitions	References

State	T_e	ω_e	$\omega_e x_e$	B_e	α_e	D_e (10^{-6} cm^{-1})	r_e (Å)	Observed Transitions: Design.	Observed Transitions: ν_{00}	References
$^{14}N_2$ (continued)										
B' $^3\Sigma_u^-$	66272.4_7	1516.88 z	12.18_1 [a]	1.473_3 [b]	0.0166_6 [c]	(5.56)	1.278_4	B'→B, R "Y" bands,[d]	6545.5 (z)	(32)(36) (182)
W $^3\Delta_u$	59808	1501.4 (z)	11.6					B'↔X,[e] R	65852.35 z	(30)* (35) (66)* (149) (155)
								Ogawa-Tanaka-Wilkinson b.		
								W↔B, R,V	73	(102)(124) (131)(157)
								Wu-Benesch b.		
B $^3\Pi_g$	59619.3_5 [g]	1733.39 z	14.122 [h]	1.6374_5 [i]	0.0179_1 [j]	[5.9]	1.2126_0	W←X,[f] R	59380	(123)* (155)
								Saum-Benesch b.		
A $^3\Sigma_u^+$	50203.6_3	1460.64 z	13.87_2 [n]	1.4546 [o]	0.0180 [p]	[6.1$_5$]	1.2866	B[k]↔A,[l] V	9552.0$_3$ z	(29)(196)
								1st pos. gr.		
X $^1\Sigma_g^+$	0	2358.57 z	14.324 [r]	1.99824_1 [s]	0.017318 [s]	[5.76]	1.09768_5	B←X,[m] R	59306.81 z	(40)
								Wilkinson b.		
								A[q]↔X,[m] R	49754.78 z	(29)(70)(85)
								Vegard-Kaplan b.		
								Rot.-vibr.[t] and rot. sp.		
								- pressure induced		(14)(59)(63) (86)(135) (141)(181)
								- el. field induced		(185)
								Raman spectra[u]		(20)(134) (167)
								Mol. beam magn. reson.[v]		

N_2: [a] $\omega_e y_e = +0.0418_6$, $\omega_e z_e = -0.000732$ (196).

[b] Spin splitting constants (v=5); $\lambda = +0.66$, $\gamma = -0.0030$ (66).

[c] $\gamma_e = +0.000009$ (196).

[d] Also referred to as "infrared afterglow bands".

[e] RKR Franck-Condon factors (75)(196). Rotational intensity distribution (120).

[f] Franck-Condon factors (123).

[g] $A_e = 42.24$ (133).

N_2 (continued):

[h] $\omega_e y_e = -0.0569$, $\omega_e z_e = +0.00361$ (196); slightly different

State	T_e	ω_e	$\omega_e x_e$	B_e	α_e	D_e (10^{-4} cm^{-1})	r_e (Å)	Observed Transitions: Design.	Observed Transitions: ν_{00}	References
$^1H^{81}Br$										DEC 1976 A
μ = 0.99542702		D_0^0 = 3.758 eV[a]				I.P. = 11.67 eV[b]				
Numerous absorption bands above 114000 cm^{-1}, tentatively assigned to higher members of two Rydberg series starting with L and M and converging to A $^2\Sigma^+$ of HBr^+; I.P.[$A^2\Sigma^+$,v=0] = 123373 cm^{-1} (15.296$_4$ eV).										(43)
M ($^1\Sigma^+$)	(109473)	[1308]	v=0...4 observed. Assigned as $4p\sigma\,4p\pi^4\,6s\sigma$.[c]					M ← X,	108814	(43)*
L ($^1\Sigma^+$,$^1\Pi$)	(104201)	[1262]	v=0...3 observed. Assigned as $4p\sigma\,4p\pi^4\,5p\sigma$ and/or $5p\pi$.[c]					L ← X,	103519	(43)*
Further absorption bands of doubtful assignment between 75200 and 83600 cm^{-1}.										(13)(15)
K[d]	1	(83902)	(2518)[e]		[8.195]		[22.0]	[1.437$_5$]	K ← X, R	83847.9[f] Z (15)
J[d]	1	(81243)	(2502)[e]		[8.02$_7$][g]		[3.6$_1$]	[1.453]	J ← X, R	81180.7[h] Z (13)*
I[d]	1	(80436)	(2525)[e]		[8.16$_9$][i]		[10.$_4$]	[1.440]	I ← X, R	80385.6[j] Z (13)*
g ($^3\Sigma^-$)0^+	t	[79253.2]			[7.6$_3$][k]		[-17]	[1.49]	g ← X, R	77940.$_0$ Z (13)* (36)*
F $^1\Delta$	t	[78322.3]			[8.20]			[1.43$_7$]	F ← X, R	77009.1 Z (36)*
f_1 $^3\Delta_1$	t	(76814)	[2299.7] Z		8.02$_7$	0.21$_3$		1.453	f_1 ← X, R	76650.9 Z (13)(36)*
D $^1\Pi$	u	(76310)	[2405.5] Z		8.12$_5$	0.21		1.444	D ← X, R	76199.4 Z (13)* (36)*
d_0 $^3\Pi_0$	u	(76193)	[2418.5] Z		[7.624][l]	(0.32)		[1.490$_4$]	d_0 ← X, R	76088.8 Z (13)(36)*
E ($^1\Sigma^+$)0^+	t	[76691]			[7.34][m]			[1.51$_9$]	E ← X, R	75378 (36)
V $^1\Sigma^+$	n	(75800)	(790)	Bands in emission above 46500 cm^{-1}, in absorption above 75700. Incomplete analysis.					V ↔ X,[o] R	(74900) (14)(36)*
f_2 $^3\Delta_2$	t	[75533.8]			[8.67$_5$][p]		[16.$_5$][p]	[1.397]	f_2 ← X, R	74220.6 Z (13)(36)*
f_3 $^3\Delta_3$	t	[75403.1]	Weak transition.		[7.41]		[-7.6]	[1.51$_2$]	f_3 ← X, R	74089.9 Z (36)*
e $^3\Sigma^+$	t	[75053]	Very diffuse, unresolved band.						e ← X, R	73740 (36)
d_1 $^3\Pi_1$	u	[74855]	Diffuse band, rotational structure unresolved.						d_1 ← X, R	73542 (13)(36)
d_2 $^3\Pi_2$	u	[74753]	Diffuse band, rotational structure unresolved.						d_2 ← X, R	73440 (13)(36)

State	T_e	ω_e	$\omega_e x_e$	B_e	α_e	D_e (10^{-4} cm^{-1})	r_e (Å)	Observed Transitions: Design.	Observed Transitions: ν_{00}	References
$^1H^{81}Br$ (continued)										
C $^1\Pi$ v	70578	2552	z 52	7.89	0.30		1.46_5	C← X,[q] R	70527.6 z	(13)(32)*
b_0 $^3\Pi_0$ 0^+ v	(68998)	[2452]		$[7.99_6]^r$			[1.455]	b_0← X, R	68911.2 z	(13)(32)*
$^3\Pi_0$ 0^- v	(68991)							R	68904[s] H	
b_1 $^3\Pi_1$ v	(67180)	[2444.2]	z	8.14_8^r	0.29_2		1.442	b_1← X, R	67088.4 z	(13)* (32)*
b_2 $^3\Pi_2$ v	[67663.0]			$[7.80_5]^r$			[1.473]	b_2← X, R	66349.8 z	(13)(32)*

[1]HBr: [a]From $D_0^0(H_2)$, $D_0^0(Br_2)$, and ΔH_{f0}(HBr; from gaseous H_2, Br_2).
[b]Average value from photoionization (10) and photoelectron spectra (23)(29); refers to X $^2\Pi_{3/2}$ of the ion. A more recent paper (39) gives 11.64_5 eV.
[c]Strongly broadened by preionization; estimated lifetime against preionization 9.5×10^{-15} s (46).
[d]I, J, K correspond to absorption bands with clear analogues in DBr.
[e]From the observed HBr-DBr isotope shift assuming that the observed bands are 0-0 bands.
[f]Band [37] of (15).
[g]Λ-type doubling, $\Delta\nu_{ef} = + 0.14_2 \times J(J+1) - \ldots$; B and D represent average values.
[h]Band [28] of (13). Sharp P, Q, R branches; the Q levels appear to be predissociated for $J \geq 14$.
[i]From R, P branches. $\Delta\nu_{ef} = - 0.041 \times J(J+1)$.
[j]Band [26] of (13).
[k]Perturbed at high J.
[l]Slightly diffuse lines.
[m]Perturbed.
[n]Derived from $H^+ + Br^-$; configuration $\ldots\sigma\pi^4\sigma^*$.
[o]Heavily perturbed extensive band system. Absorption lines above 75923 cm^{-1} are diffuse. B' varies irregularly between 3.4 and 4.5 cm^{-1}.
[p]Average values for the two Λ-type doubling components.
[q]Very strong absorption, lines are diffuse.
[r]Diffuse rotational structure.
[s]Diffuse Q head.
[t]Configuration $\ldots\sigma^2\pi^3 5p\pi$.
[u]Configuration $\ldots\sigma^2\pi^3 5p\sigma$.
[v]Configuration $\ldots\sigma^2\pi^3 5s\sigma$.

State	T_e	ω_e	$\omega_e x_e$	B_e	α_e	D_e (10^{-4} cm^{-1})	r_e (Å)	Observed Transitions: Design.	Observed Transitions: ν_{00}	References
$^1H^{81}Br$ (continued)										
A ($^1\Pi$) w		Continuous absorption starting at ~35000 with maximum at 56400 cm^{-1}.								
X $^1\Sigma^+$ 0		2648.975^x	Z 45.217_5^y	8.46488_4^x	0.23328^z	3.457_5 [a']	1.41443_5	A ← X		(1)(2)(4)(5)(28)
								Rot.-vibr. sp. [b'c']		(21)
								Rotation spectrum [d'c']		(8)(17)(31)
								Raman sp. [e']		(45)
								Mol. beam el. reson. [f']		(42)

^{1}HBr (continued):

[w] Configuration $\ldots\sigma^2\pi^3\sigma^*$.

[x] These are Y_{10} and Y_{01} values; applying Dunham corrections (21) obtain $\omega_e = 2649.21_5$, $B_e = 8.46506_5$. Additional corrections (adiabatic, non-adiabatic) are discussed by (38). The microwave B_0 value of (17) was included in the evaluation of B_e. See also [b'f'].

[y] $\omega_e y_e = -0.0029$.

[z] $+ 0.000873_5(v+\frac{1}{2})^2 - 0.000120(v+\frac{1}{2})^3$.

[a'] $- 0.039_7 \times 10^{-4}(v+\frac{1}{2}) + 0.0038(v+\frac{1}{2})^2$;

[b'] $H_v = 7.63 \times 10^{-9} - 0.55 \times 10^{-9}(v+\frac{1}{2})$.

In absorption the 1-0, 2-0, 3-0, 3-1, 4-0, 5-0, 6-0 bands have been studied (6)(7)(12)(21)(41); in emission 1-0, 2-1, 3-2, 4-3 (11)(20). The constants in the table are from (21), those of (20)(41) are very similar and of comparable accuracy. See also (47). Absolute intensities have been measured (16)(18)(30)(33) and the dipole moment function has been calculated; (40) give for $H^{79}Br$ [D,Å]; $\mu_{e\ell}(r) = +0.788 + 0.315(r-r_e) + 0.575(r-r_e)^2$; see also (24)(34)(37).

[c'] For observations and measurements of pressure-induced bands and pure rotation lines ($\Delta J=2$) see (22)(27). The pressure broadening of the lines has been studied by (16)(25).

[d'] Absolute intensities have been measured by (19).

[e'] Raman cross sections in gaseous HBr.

[f'] The following constants (as well as corresponding values for $H^{79}Br$) are given in (42):

- $\mu_{e\ell}(v=0,J=1) = 0.8265$ D [in a later paper (44) derive 0.8282 D from Stark effect of rotation spectrum];
- quadrupole and other hyperfine coupling constants;
- $g_J = 0.3712$.

These constants supersede earlier values of (9)(17)(26)(31)(35).

State	T_e	ω_e	$\omega_e x_e$	B_e	α_e	D_e (10^{-4} cm^{-1})	r_e (Å)	Observed Transitions: Design.	Observed Transitions: ν_{00}	References
$^2H^{81}Br$		μ = 1.96518641	D_0^0 = 3.804 eV[a]		I.P. = 11.67$_3$ eV[b]					DEC 1976 A
		Numerous absorption bands above 114000 cm^{-1}, see ^{1}HBr.								(13)
M ($^1\Sigma^+$)	(109374)	[1000] v=0...5 observed. } See ^{1}HBr.						M ← X,	108937	(13)*
L ($^1\Sigma^+$,$^1\Pi$)	(104141)	[971] v=0...4 observed. }						L ← X,	(103690)	(13)*
		Further absorption bands of doubtful assignment between 72000 and 83800 cm^{-1}.								(6)
K[c] 1	(83908)	(1792)[d]		[4.121][e]		[0.80]	[1.442$_8$]	K ← X, R	83867.1[f] Z	(6)
J[c] 1	(81248)	(1781)[d]		[4.083][g]		[1.36]	[1.449$_5$]	J ← X, R	81202.2[f] Z	(6)*
I[c] 1	(80442)	(1797)[d]		[4.107]		[1.38]	[1.445$_2$]	I ← X, R	80403.8[f] Z	(6)
g ($^3\Sigma^-$)0$^+$	(78125)	[1440.$_6$] Z		[3.79]	(0.40)[h]	[14]	[1.50$_4$]	g ← X, R	77908.8 Z	(6)(10)
F $^1\Delta$	[77989.0]			[4.095]			[1.447$_3$]	F ← X, R	77052.3 Z	(6)(10)
f_1 $^3\Delta_1$	(76787)	[1657.3] Z		4.06$_4$	0.07$_6$		1.453	f_1 ← X, R	76679.2 Z	(6)(10)
D $^1\Pi$	(76280)	[1732.6] Z		4.128[i]	0.076		1.441$_5$	D ← X, R	76209.1 Z	(6)(10)*
d_0 $^3\Pi_0$	[77027.4]			[3.99$_3$][j]			[1.466]	d_0 ← X, R	76090.7 Z	(10)*
E ($^1\Sigma^+$)0$^+$	(75682)	[1365] Z		[3.953]	(0.78)[h]		[1.472$_9$]	E ← X, R	75428.1 Z	(6)(10)
V $^1\Sigma^+$		Extensive absorption system above 75700 cm^{-1}, incompletely analysed because of strong perturbations. B_v values range from 1.68 to 2.12.						V ← X, R		(10)
f_2 $^3\Delta_2$	(74370)	[1660.3] Z		4.29$_4$	0.097	[2.4]	1.413	f_2 ← X, R	74263.1 Z	(6)(10)*
f_3 $^3\Delta_3$	[75088.6]	Weak transition.		[3.83]		[-2.1]	[1.49$_7$]	f_3 ← X, R	74151.9 Z	(10)*
e $^3\Sigma^+$	[74677]	Very diffuse, unresolved band.						e ← X,	73740	(10)
d_1 $^3\Pi_1$	[74499]	Diffuse band, rotational structure unresolved.						d_1 ← X, R	73562	(6)(10)
d_2 $^3\Pi_2$	[74391.5]			[3.906][k]		[0.36]	[1.482]	d_2 ← X, R	73454.8 Z	(6)(10)*
C $^1\Pi$	70563	1811.2 Z 25.5		4.02[l]	0.10$_5$		1.46$_1$	C ← X, R	(70501) H[q]	(6)(8)*

State	T_e	ω_e	$\omega_e x_e$	B_e	α_e	D_e (10^{-4} cm^{-1})	r_e (Å)	Observed Transitions: Design.	Observed Transitions: ν_{00}	References
$^2H^{81}Br$ (continued)										
b_0 $^3\Pi_0$ 0^+	[69837.1]			[4.08_2]^m			[1.450]	$b_0 \leftarrow X$,	R 68900.4 Z	(6)* (8)*
$^3\Pi_0$ 0^-	[69832]	Unresolved Q branch, assignment uncertain.							R (68895)	
b_1 $^3\Pi_1$	67113.$_9$	1814	Z 27	4.10^n	0.09		1.44_6	$b_1 \leftarrow X$,	R 67077.5 Z	(6)(8)
b_2 $^3\Pi_2$	[67290.7]			[4.01_8]^m			[1.461]	$b_2 \leftarrow X$,	R 66354.0 Z	(6)(8)
A ($^1\Pi$)		Continuous absorption beginning at ~39000 cm^{-1}.						A $\leftarrow$ X,		(1)
X $^1\Sigma^+$	0	1884.75	Z 22.71$_8$[o]	[4.245596]^p	0.083$_8$	[0.8832]^p	1.4145	Rot.-vibr. sp.^{q}		(2)(5)
		'837.53 = 1884.75 - 2(23.71)						Rotation spectrum^r		(3)(4)(9)(12)

^{2}HBr: [a] From D_0^0(^{1}HBr).
[b] From the photoelectron sp. (11) of the isotopic mixture.
[c] See [d] of ^{1}HBr.
[d] See [e] of ^{1}HBr.
[e] Λ-type doubling, $\Delta\nu_{ef} \approx + 0.0371\,J(J+1)$.
[f] Bands {35}, {27}, {26} of (6).
[g] Ω-type doubling, $\Delta\nu_{ef} = + 0.0314\,J(J+1)$.
[h] v=0 and 1 only; v=1 is perturbed.
[i] From P, R branches. $B_0(Q) = 4.109$.
[j] From P, R branches. $B_0(Q) = 3.92_6$.
[k] Branches are slightly diffuse.
[l] Diffuse rotational structure; v=0...4.
[m] Slightly diffuse lines.
[n] v=2, 3 diffuse. Slightly diffuse lines for v=0, 1.
[o] $\omega_e y_e = - 0.010_6$.
[p] Microwave value (9)(12).
[q] 1-0, 2-0, 3-0 bands in absorption (2), Δv=1 sequence in emission (5).
[r] $\mu_{e\ell}$(v=0) = 0.8233 D from Stark effect of 1-0 line (12).
Quadrupole and other hyperfine coupling const. (7)(9)(12).

(1) See ref. (1) of ^{1}HBr.
(2) Keller, Nielsen, JCP 22, 294 (1954).
(3) Palik, JCP 23, 217 (1955).
(4) Cowan, Gordy, PR 111, 209 (1958)
(5) See ref. (11) of ^{1}HBr.
(6) See ref. (15) of ^{1}HBr.
(7) See ref. (26) of ^{1}HBr.
(8) See ref. (32) of ^{1}HBr.
(9) De Lucia, Helminger, Gordy, PR A 3, 1849 (1971).
(10) See ref. (36) of ^{1}HBr.
(11) See ref. (39) of ^{1}HBr.
(12) See ref. (44) of ^{1}HBr.
(13) See ref. (43) of ^{1}HBr.

TABLE 16.3
van der Waals constants for various substances.

Species	$a/\text{dm}^6\cdot\text{bar}\cdot\text{mol}^{-2}$	$a/\text{dm}^6\cdot\text{atm}\cdot\text{mol}^{-2}$	$b/\text{dm}^3\cdot\text{mol}^{-1}$
Helium	0.034598	0.034145	0.023733
Neon	0.21666	0.21382	0.017383
Argon	1.3483	1.3307	0.031830
Krypton	2.2836	2.2537	0.038650
Hydrogen	0.24646	0.24324	0.026665
Nitrogen	1.3661	1.3483	0.038577
Oxygen	1.3820	1.3639	0.031860
Carbon monoxide	1.4734	1.4541	0.039523
Carbon dioxide	3.6551	3.6073	0.042816
Ammonia	4.3044	4.2481	0.037847
Methane	2.3026	2.2725	0.043067
Ethane	5.5818	5.5088	0.065144
Ethene	4.6112	4.5509	0.058199
Propane	9.3919	9.2691	0.090494
Butane	13.888	13.706	0.11641
2-Methyl propane	13.328	13.153	0.11645
Pentane	19.124	18.874	0.14510
Benzene	18.876	18.629	0.11974

$a = 2.3026\ \text{dm}^6\cdot\text{bar}\cdot\text{mol}^{-2}$ and $b = 0.043067\ \text{dm}^3\cdot\text{mol}^{-1}$ for methane. If we divide Equation 16.5 by $\overline{V} - b$ and solve for P, we obtain

$$\begin{aligned} P &= \frac{RT}{\overline{V} - b} - \frac{a}{\overline{V}^2} \\ &= \frac{(0.083145\ \text{dm}^3\cdot\text{bar}\cdot\text{mol}^{-1}\cdot\text{K}^{-1})(273.15\ \text{K})}{(0.250\ \text{dm}^3\cdot\text{mol}^{-1} - 0.043067\ \text{dm}^3\cdot\text{mol}^{-1})} - \frac{2.3026\ \text{dm}^6\cdot\text{bar}\cdot\text{mol}^{-2}}{(0.250\ \text{dm}^3\cdot\text{mol}^{-1})^2} \\ &= 72.9\ \text{bar} \end{aligned}$$

By comparison, the ideal-gas equation predicts that $P = 90.8$ bar. The prediction of the van der Waals equation is in much better agreement with the experimental value of 78.6 bar than is the ideal-gas equation.

The van der Waals equation qualitatively gives the behavior shown in Figures 16.3 and 16.4. We can rewrite Equation 16.5 in the form

$$Z = \frac{P\overline{V}}{RT} = \frac{\overline{V}}{\overline{V} - b} - \frac{a}{RT\overline{V}} \tag{16.6}$$

TABLE 16.4
The Redlich-Kwong equation parameters for various substances.

Species	$A/\text{dm}^6\cdot\text{bar}\cdot\text{mol}^{-2}\cdot\text{K}^{1/2}$	$A/\text{dm}^6\cdot\text{atm}\cdot\text{mol}^{-2}\cdot\text{K}^{1/2}$	$B/\text{dm}^3\cdot\text{mol}^{-1}$
Helium	0.079905	0.078860	0.016450
Neon	1.4631	1.4439	0.012049
Argon	16.786	16.566	0.022062
Krypton	33.576	33.137	0.026789
Hydrogen	1.4333	1.4145	0.018482
Nitrogen	15.551	15.348	0.026738
Oxygen	17.411	17.183	0.022082
Carbon monoxide	17.208	16.983	0.027394
Carbon dioxide	64.597	63.752	0.029677
Ammonia	87.808	86.660	0.026232
Methane	32.205	31.784	0.029850
Ethane	98.831	97.539	0.045153
Ethene	78.512	77.486	0.040339
Propane	183.02	180.63	0.062723
Butane	290.16	286.37	0.08068
2-Methyl propane	272.73	269.17	0.080715
Pentane	419.97	414.48	0.10057
Benzene	453.32	447.39	0.082996

where A, B, α, and β, are parameters that depend upon the gas. The values of A and B in the Redlich-Kwong equation are listed in Table 16.4 for a variety of substances. The parameter α in the Peng-Robinson equation is a somewhat complicated function of temperature, so we will not tabulate values of α and β. Equations 16.7 and 16.8, like the van der Waals equation (Example 16–2), can be written as cubic equations in $\overline{V}$. For example, the Redlich-Kwong equation becomes (Problem 16–26)

$$\overline{V}^3 - \frac{RT}{P}\overline{V}^2 - \left(B^2 + \frac{BRT}{P} - \frac{A}{T^{1/2}P}\right)\overline{V} - \frac{AB}{T^{1/2}P} = 0 \qquad (16.9)$$

Problem 16–28 has you show that the Peng-Robinson equation of state is also a cubic equation in $\overline{V}$.

EXAMPLE 16–3
Use the Redlich-Kwong equation to calculate the molar volume of ethane at 300 K and 200 atm.

AN 014.S20

MEASUREMENT OF THE REDUCTION OF POTASSIUM FERRICYANIDE BY L-ASCORBIC ACID WITH A SHIMADZU UV-1700 SPECTROPHOTOMETER USING A STOPPED-FLOW ACCESSORY.

The reduction of Potassium Ferricyanide by Ascorbic Acid is a well known kinetic reaction that was first published by Tonomura *et al.*[1] The speed of this reaction is dependent on the pH value of the solution which makes this reaction a very useful one for testing the performance of kinetic instruments

Keywords: Stopped-Flow Accessory, Shimadzu UV-1700, Rapid Kinetics

Introduction

When Potassium Ferricyanide ($K_3Fe(CN)_6$) is dissolved and brought into solution with L-Ascorbic Acid (Vitamin C, $C_6H_8O_6$), the Ferricyanide ($Fe(CN)_6^{3-}$) can be reduced by the Ascorbic Acid (AA) to form $Fe(CN)_6^{4-}$. Being an acid AA is present in the solution in the form of AA, AA^- and AA^{2-}, the ratio of these depending on the pH of the solution

$$AA \leftrightarrow AA^- + H^+$$

$$AA^- \leftrightarrow AA^{2-} + 2H^+$$

This also means that the speed of the reaction is determined by the pH of the solution. Two of the forms in which AA is present in the solution, AA^- and AA^{2-}, can react with Ferricyanide

Methodology

The reaction mechanisms for the reduction of Ferricyanide by Ascorbic Acid are

$$AA^- + Fe(CN)_6^{3-} \xrightarrow{k_1} AA\cdot + Fe(CN)_6^{4-}$$

and

$$AA\cdot + Fe(CN)_6^{3-} \xrightarrow{k_2} AA^\circ + Fe(CN)_6^{4-} + H^+$$

for the AA^- form and

$$AA^{2-} + Fe(CN)_6^{3-} \xrightarrow{k_3} AA^- \cdot + Fe(CN)_6^{4-}$$

and

$$AA^- \cdot + Fe(CN)_6^{3-} \xrightarrow{k_4} AA^\circ + Fe(CN)_6^{4-}$$

for the AA^{2-} form. In these equations AA° is the oxidised form of AA, $C_6H_6O_6$.

The free radicals formed in this reaction instantaneously react with $Fe(CN)_6^{3-}$ and only k_2 and k_4 contribute to the pseudo first order rate constant k, which can be used if $[AA] >> [Fe(CN)_6^{3-}]$. The concentration of $Fe(CN)_6^{3-}$ during the reaction is then given by

$$[Fe(CN)_6^{3-}] = [Fe(CN)_6^{3-}]_0 \cdot \exp^{-kt}$$

Experimental

Potassium Ferricyanide has an absorbance maximum at 420 nm, this can be seen in the spectrum of $K_3Fe(CN)_6$ shown in Figure 1.

All kinetic traces were collected at this wavelength with an AA syringe solution concentration of 20 mM and a $Fe(CN)_6^{3-}$

concentration of 1 mM in the syringes. The experiments were performed at room temperature and the pH value was determined by the Ascorbic Acid concentration (pH = 3)

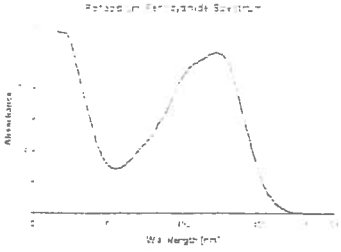

Figure 1: Spectrum of $K_3Fe(CN)_6$

First the acquisition process was started on the Shimadzu UV-1700 spectrophotometer and subsequently the syringes on the SFA-20 were pushed by hand to start the reaction in the cell between Ferricyanide and Ascorbic Acid. The SFA-20 stopped-flow accessory used for these measurements with the Shimadzu UV-1700 was equipped with a standard cell. Kinetic traces were collected for 10 seconds with a time resolution of 100 ms per data point and 101 data points in total were recorded for every trace.

Results

Traces of 14 separate experimental shots were recorded with very good reproducibility. This can be seen in Figure 2 where all the individual traces are shown for the first 3.5 seconds only, because the reaction was over after 3-4 seconds.

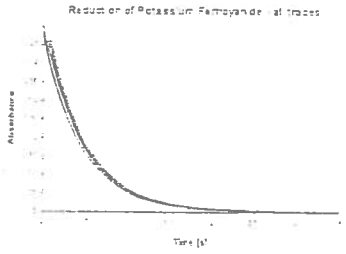

Figure 2: All kinetic traces collected for the reduction of $K_3Fe(CN)_6$

A single trace was then used to fit first order reaction kinetics. Both the original data and the fit to the data are shown in Figure 3.

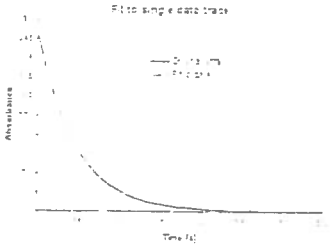

Figure 3: Kinetic trace for $K_3Fe(CN)_6$ reduction with a fit to the data

The first order rate constant found for the reaction was k = 2.15 s^{-1} which is in good agreement with the value found in the literature[1].

Conclusion

The first order kinetics assumption provides a very good fit to the original data, proving that it was safe to make this assumption with the used concentrations of reagents. Also the quality of the data collected with the Shimadzu UV-1700 spectrophotometer was very good and consistent. These experiments therefore prove that the Shimadzu UV-1700 is a very suitable spectrophotometer to measure fast kinetic reactions reliably in conjunction with the SFA-20 stopped-flow accessory.

References

[1] B. Tonomura *et al*., Analytical Biochemistry 84 (1978) 370-383

Acknowledgements

We would like to thank Shimadzu U.K. for making the UV-1700 available to us for measurements

Hi-Tech Scientific contacts:

General Manager: Victor Higgs

Technical Manager: Ted King

Sales Office Manager: David Mitchell

Technical Sales Engineer: Melanie Nijman

HI-TECH SCIENTIFIC

Hi-Tech Scientific, Brunel Road, Salisbury SP2 7PU. United Kingdom

Telephone: National 01722 432320

International +44 1722 432320 USA Toll Free 1 800 334 0724

Facsimile: National 01722 432324 International +44 1722 432324

EXPERIMENT 41

Computational Determination of the Molecular Constants of HCl

Objective

Calculation of the molecular constants of HCl using ab initio quantum mechanical methods.

Introduction

Experiment 36 guides you through the acquisition and analysis of the infrared spectrum of gaseous HCl with the goal of obtaining its molecular constants. It is helpful to review here the ultimate objective of that experiment in terms of the five molecular constants sought. These constants are (1) the harmonic frequency, $\tilde{\nu}_e$; (2) the anharmonicity constant, $\tilde{\nu}_e\chi_e$; (3) the rotational constant, B_e; (4) the rotation–vibration coupling constant, α_e; and (5) the centrifugal distortion constant, D.

This experiment has the same objective. However, you will not use a traditional "experimental" approach that relies on getting data from a spectrophotometer; instead you will employ computational methods that are based on quantum chemistry. The term "ab initio" cited in the Objective means "from the beginning," and it may be interpreted that you will obtain these results from an entirely mathematical quantum mechanical calculation. The goal of these approaches is to obtain solutions to the Schrödinger equation by making as few approximations as possible and by avoiding the use of adjustable parameters.

You will use some of the most advanced and reliable techniques currently available in standard computational chemistry applications. The methods to be used do not rely on any expeditious assumptions (or adjustable parameters) to facilitate or even permit the calculations to be made. Moreover, these calculations can be performed on a stand-alone personal computer. Thus, you are the beneficiary of forty years of research in quantum chemistry, immense advancements in computing power, and the successful efforts of computer programmers.

The quality of the results that can be achieved for small molecules (such as diatomics) using advanced quantum chemical calculations permits one to determine molecular constants to within one percent of the experimental quantities. This achievement is particularly significant because one can now calculate the molecular constants and thus predict the rotational–vibrational spectra of unstable or exotic species.

Computational Approach

Before we present the computational details, we will give you the basic outline of the approach to be followed in this experiment. The strategy is to obtain the internuclear potential energy (PE) function of HCl in the vicinity of the potential minimum, for it is the shape of the PE function in this region that determines the five molecular constants mentioned. Figure 1 shows a qualitative example of the PE function of a diatomic molecule and the portion of the curve that we strive to calculate.

In *Step 1*, we will use high-level quantum chemical methods to calculate the electronic energy of HCl at specifically chosen internuclear separations. Then in *Step 2* we will refine these energies using a computational technique called *basis set extrapolation*. In *Step 3* we will fit these refined PE points to a sixth-order

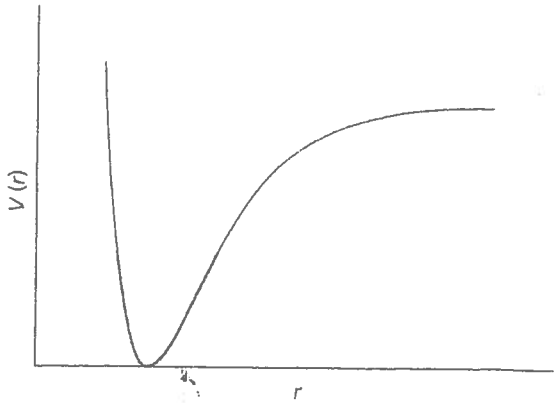

Figure 1. Qualitative potential energy curve for a diatomic molecule. The section of the curve that we will calculate is highlighted.

power series as a function of the internuclear distance. Finally, in *Step 4* we will use coefficients of this power series to obtain the sought-after five molecular constants. We will assess the quality of the computational results by comparing them with their experimental counterparts.

You will use a high-level method for obtaining the electronic energy of HCl called coupled cluster with single, double, and perturbative triple excitations—abbreviated CCSD(T).[1] This method is perhaps the most reliable approach available that takes into account the correlated interactions of electrons. The basis set used in the calculations represents the molecular orbitals. It consists of an array of analytical functions centered on the H and Cl atoms and attempts to capture the "true" molecular wavefunction. We would like to use a basis set that is as large as possible, providing sufficiently extensive spatial "coverage" of electronic motion around the HCl molecule. Ideally this representation requires an infinite number of basis functions, but this is clearly impractical. To approximate this goal, however, we will perform three PE calculations for each chosen H–Cl separation with basis sets possessing increasing numbers of functions. These basis sets belong to a family called augmented correlation-consistent polarized valence functions, abbreviated aug-cc-pVXZ,[2] where X denotes a quantity called zeta. In this experiment, zeta will be double, triple, and quadruple (or $X = 2$, 3, and 4). As zeta gets larger, additional functions are used, increasing both the compactness (tightness) and spatial extent (size) of the basis set. The energies calculated from these larger basis sets come therefore incrementally closer to the energy that would be obtained in the limit of infinitely extensive basis functions. We will estimate this limiting energy by performing an extrapolation of the energies obtained with $X = 2$, 3, and 4 basis sets. This extrapolation yields an estimate of the energy in the *complete basis set* (CBS) limit.

Test Run of a CBS-Limit Calculation

Before you get started with the HCl calculations we will guide you through a CBS extrapolation of the electronic energy of helium. We choose this example because the calculations are very fast. You will also be able to see how the energy changes with increasing zeta and will be able to compare the CBS-extrapolated result of the helium ground state energy with the experimental value.

The calculations described in this experiment can be performed using Gaussian 03 for Windows (G03W) or earlier versions. This is a suite of programs that can be used to carry out a wide range of computational objectives on the Microsoft Windows platform. The work outlined here can be carried out on a PC with typical RAM memory and disk storage space. The text you enter into the

input file sections of the G03W file appears in typewriter font and the relevant parts of the output file are shown here in smaller font. **Underlined boldface** text denotes what you will see in the G03W input file.

Enter the following text in the **Route Section** (Gaussian input is case insensitive):

```
ccsd/cc-pvdz
```

We perform a CCSD calculation because with only two electrons there are no triple excitations. In the **Title Section** section, add whatever text you like to document your calculation.

The **Charge & Multicipl.** ("multicipl." is how G03W abbreviates "multiplicity") window is the place where you enter the charge of the species followed by its spin multiplicity, here,

```
0,1
```

The He atom is neutral; thus its charge is zero. This calculation is on the ground state, so the electrons are spin-paired, and the total spin quantum number, S, is zero. The multiplicity $(2S + 1)$ is therefore 1.

Next is the **Molecule Specification**, which contains simply the symbol of the helium atom (no coordinates are needed).

Calculations

The CCSD energy is found at the end of the output file. For the CCSD/cc-pVDZ calculation, the result we seek can be found at the bottom of the Gaussian output file in the section called the archive. The archive looks like this (the CCSD information is in boldface):

N-N = 0.000000000000D + 00 E-N = −6.737201240703D + 00 KE = 2.855176138096D + 00
1|1|UNPC-UNK|SP|RCCSD-FC|CC-pVDZ|He1|PCUSER|02-Dec-2005|0||#CCSD/CC-PV
DZ||He ccsd double zeta||0,1|He||Version = x86-Win32-G98RevA.9|HF = −2.855
1605|MP2 = −2.8809888|MP3 = −2.8863612|MP4D = −2.887507|MP4DQ =
−2.8873895|MP4
SDQ = −2.8873903|CCSD = −2.8875948|RMSD = 7.972e-011|PG = KH||@

The CCSD energy, −2.8875948, is in atomic units (hartrees). This energy represents the ΔE for the process

$$\mathrm{He}^{2+} + 2e^- \rightarrow \mathrm{He}. \tag{1}$$

Repeat the CCSD calculation using the cc-pVTZ and cc-pVQZ basis sets. Copy the three coupled cluster energies from the Gaussian output files into a spreadsheet that supports user-defined regression analysis, such as Excel/SDAS. Arrange the data in a three-row column containing the double, triple, and quadruple energies. Enter the numbers 2, 3, and 4 in the cells to the left of these entries, respectively.

The extrapolation function you will use to obtain the CBS energy consists of an exponential and a Gaussian term:

$$E(X) = E_{\mathrm{CBS}} + be^{-(X-1)} + ce^{-(X-1)^2}. \tag{2}$$

Fit your observed CCSD energies for X = 2, 3, and 4 to equation (2) with a nor linear fit to extract the value of E_{CBS}. A plot of the CCSD energy versus X shown in Figure 2. You should obtain a value of −2.90344 hartrees.

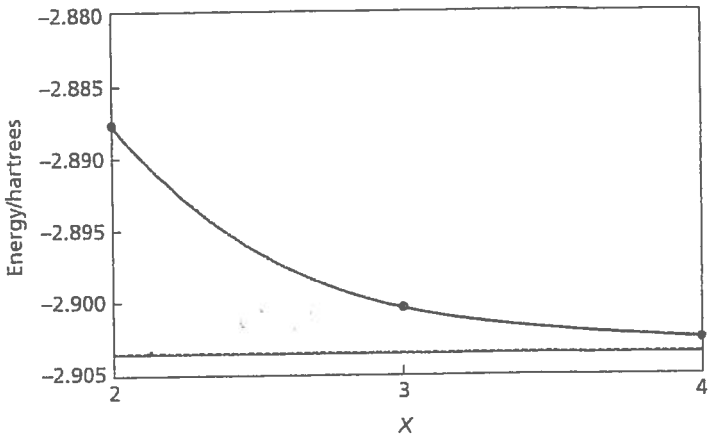

Figure 2. Extrapolation of the CCSD(T)/cc-pV*X*Z energies of helium to the CBS limit using the function in equation (2). The dotted line represents the value of E_{CBS}; the solid line is the experimental value the total helium energy.

Now compare your CCSD/CBS energy of helium with the experiment. Tl first two ionization energies (experimental) of helium, reported to be 24.5874 ar 54.416 electron volts (eV), respectively, correspond to the processes

$$He \rightarrow He^+ + e^- \quad (3$$

and

$$He^+ \rightarrow He^{2+}\ e^-. \quad (3$$

Consider the process in equation (1) and compare your calculated energy with tl sum of these ionization energies. Use the conversion factor 1 h = 27.211396 e What is the percent error in your CCSD(T)/CBS energy?
Now on to HCl.

Step 1

Obtain the CCSD(T) energies for HCl at internuclear distances between 0.8 Å 1.8 Å. This type of calculation is called a *potential energy scan*. Enter the fo lowing text in the Route Section:

```
ccsd(t)/aug-cc-pvdz     scan
```

In these calculations we will use the augmented correlation-consistent basis se The `scan` entry is a keyword that instructs the program that a variable (in tl case the H–Cl distance) will be incremented.

Add some text to the Title Section, e.g., `HCl scan double zeta, a` type `0,1` in the Charge & Multicipl. box. For the Molecule Specification sectic enter

```
H
Cl    1      r

r     1.0    8    0.1
```

The second line indicates that the Cl atom is attached to atom 1 (H) at a distance r. The third line is blank. The last line, used in concert with the scan keyword, tells the program to start with a value of r = 1.0 Å, perform the calculation indicated in the Route Section, then increment r by 0.1 Å, and repeat the calculation. This process is carried out for a total of eight 0.1-Å steps, thus producing a scan consisting of 9 points along the H–Cl internuclear potential energy surface.

After this calculation, carry out two additional scans using the triple and quadruple zeta basis sets. Simply replace the "d" in the basis set in the Route Section by "t" and then "q". The other parts of the input file remain the same (except for the entries in the Title Sections).

Step 2

Now we will use the results from Step 1 to obtain the CBS-extrapolated energies for *each* of the nine points along the PE curve. Although the results of the scan are summarized in the Gaussian output file, the energies reported there are unfortunately not formatted to sufficient significant figures. Therefore you will have to copy the numerical results from the very end of the file, paste them into a word processor, and arrange them in a single, continuous line with the values separated by commas (don't worry about soft line returns). The results of the double zeta scan, as they appear in the output file, are shown in the Appendix of this experiment. Save this data as an ASCII-delimited text file. Import the file to Excel/SDAS, using the commas to delimit the values from each other so that they occupy separate cells in a row. In a similar fashion, transfer the CCSD(T) data from the triple and quadruple zeta scans to this spreadsheet so that the three energies for a given H–Cl distance are aligned in a column. Enter the numbers 2, 3, and 4 into another column, and use SDAS to obtain the CBS energies for each H–Cl scan point, just as you did in the exercise with helium. This process is less tedious than it might seem because SDAS recalls the user-defined function during a session. You can use the same values—$E_{CBS} = -409$ and $b = c = 1$—for the initial guesses of the parameters in these analyses.

After you complete each CBS extrapolation, copy the CBS energy from the SDAS *Model* sheet and paste it into your working spreadsheet (you must use *Paste Special—Values*). Arrange these CBS values in a column. Enter the respective H–Cl distances (in Å units) in the cells to the left of the CBS energies. Plot your data; if all went well, your graph should resemble the bold portion of the curve in Figure 1.

Step 3

Fit your (E,r) data to the sixth-order polynomial

$$E(r) = a_0 + a_2(r - r_e)^2 + a_3(r - r_e)^3 + a_4(r - r_e)^4 + a_5(r - r_e)^5 + a_6(r - r_e)^6, \quad (4)$$

which has seven parameters. The reason that we use such an extensive function is that it is able to capture accurately the curvature of the PE function in the vicinity of the minimum and thus yield accurate values of the desired molecular constants. The first parameter, a_0, sets the energy at the minimum of the function, where $r = r_e$. The second-order constant, a_2, accounts for the harmonic (parabolic) character of the PE function, and the remaining constants describe the anharmonic quality of the potential. As we will see in Step 4, the molecular constants can be extracted from these constants.

Fit your CBS scan energies to equation (4). You will probably need initial guess values of the parameters. You can easily estimate a_0 and r_e from the position of

the minimum of your plotted curve, and it is safe to use initial guesses of zero for a_3 and higher. To estimate a_2, look at your plot and see how much the energy increases for a change in r of 0.1 Å from r_e; the increase is approximately $a_2(0.1)^2$.

Step 4

Finally you have to extract the HCl molecular constants from the fitted parameters. To do so, you must first convert the fitted coefficients a_2, a_3, and a_4 to cgs units. Look carefully at equation (4) and identify the units that these coefficients currently have. Then convert them so that they use energy units of ergs and length units of cm; 1 Å $= 10^{-8}$ cm and 1 hartree $= 4.3597482 \times 10^{-11}$ erg.

Because the experimental spectroscopic constants with which you will compare values were obtained for $^1H^{35}Cl$, you should use the appropriate isotopic masses of 1.007825032 and 34.96885271 atomic mass units, respectively.[3] The reduced mass is $\mu = m_H m_{Cl}/(m_H + m_{Cl})$.

The first constant, r_e, comes directly from the fit to equation (4). For the other constants, we are guided by the treatment presented by Herzberg:[4]

1. The rotational constant is determined from the average moment of inertia, $I = \mu\langle r\rangle^2$, of the molecule. It controls the spacings between rotational levels and is given by

$$B_e = \frac{h}{8\pi c \mu r_e^2}. \tag{5}$$

2. The vibrational frequency $\tilde{\nu}_e$ is the natural frequency of vibration of the atoms connected by the "spring" of the chemical bond. It is determined by the stiffness of the spring and the masses of the atoms. It is related to a_2 by

$$\tilde{\nu}_e = \frac{1}{2\pi c}\sqrt{\frac{2a_2}{\mu}}. \tag{6}$$

3. Because the potential energy curve is not a true parabola, as the vibrational quantum number increases the average bond length and therefore the moment of inertia also increases. This change is described by the rotational–vibrational coupling constant α_e, given by

$$\alpha_e = -\frac{6\dot{B}_e^2}{\tilde{\nu}_e}\left(\frac{a_3 r_e}{a_2} + 1\right). \tag{7}$$

4. The molecular spring is not infinitely stiff, so as the molecule rotates faster and faster, the inertia of the atoms (or the "centrifugal force") causes the bond to stretch, increasing the moment of inertia and decreasing the spacings between rotational energy levels. This effect is controlled by spring stiffness and the masses, and the associated centrifugal distortion constant D is given by

$$D = \frac{4B_e^3}{\tilde{\nu}_e^2}. \tag{8}$$

5. The anharmonicity constant $\tilde{\nu}_e\chi_e$ describes the deviation of the potential energy curve from a parabola. Because the true PE curve becomes wider faster than a parabola does as r increases, the spacings between the vibrational levels become smaller. The decrease in vibrational spacing with

increasing quantum number is described by the anharmonicity constant $\tilde{\nu}_e\chi_e$. It can be calculated from your fit through

$$\tilde{\nu}_e\chi_e = \frac{B_e}{8}\left[15\left(1 + \frac{\alpha_e\tilde{\nu}_e}{6B_e^2}\right)^2 - \frac{12a_4r_e^2}{a_2}\right]. \quad (9)$$

Tabulate your molecular constants and compare them with the values reported in Herzberg.[3]

Questions and Further Thoughts

1. If you were going to obtain the molecular constants for DCl ($^2H^{35}Cl$), explain why you would not have to repeat the ab initio calculations (or even the polynomial fit). How, then, would you proceed to obtain the results?

2. A mathematical function that qualitatively describes real diatomic potential curves is the Morse potential,

$$E(r) = D_e\{1 - \exp[-\beta(r - r_e)]\}^2 + C, \quad (10)$$

where D_e is the dissociation energy, β is a constant that determines the curvature, r_e is the position of the minimum, as before, and C is the energy at the potential minimum (see Figure 1). Fit your ab initio data to a Morse potential. You can use the r_e value you read from your potential curve for an initial guess. D_e gives the strength of the molecular bond; since your data cover only a relatively small region near the bottom of the well, a reasonable initial guess for D_e is two times the range of energies you obtained in your scan. The Morse function indicates that β must have units of inverse length; $1/\beta$ is the characteristic length over which the potential energy curve "leans over" and begins to approach its asymptote, so 1 $Å^{-1}$ is a reasonable initial guess for β. $C + D_e$ is the energy of the separated H and Cl atoms; for the calculation you have done, -460 hartrees is a workable guess for C. Compare the fitted values of r_e and D_e with those in the literature,[2,3] and comment. Does your estimate of D_e, in particular, agree well? What would you have to do to get a better computational estimate?

3. What is the uncertainty in your value of the harmonic frequency, $\tilde{\nu}_e$? Use the standard deviation of a_2—see the *Model* sheet from your regression analysis.

4. If you want to calculate the molecular constants for an uncommon molecule, try something like $^2H^3H$ or $^3H^3H$.

5. The ionization energy of the helium cation (a one-electron atom) can be calculated exactly from the Schrödinger equation. Its value is -2 hartrees.[6] Determine this value from a CCSD/CBS calculation of He^+ (charge 1, multiplicity 2) and your CCSD/CBS energy of the neutral atom. See processes (1), (3a), and (3b). Compare your result with the experimental value.

Notes

1. See I. N. Levine, *Quantum Chemistry,* 5th ed., pp. 568–573, Prentice Hall (Upper Saddle River, NJ), 2000.
2. I. N. Levine, op cit., p. 492.
3. http://physics.nist.gov/PhysRefData/Compositions/
4. G. Herzberg, *Spectra of Diatomic Molecules,* 2nd ed., pp. 66–82, 90–97, 103–115, Van Nostrand Reinhold (New York), 1950.
5. G. Herzberg, op. cit., p. 534; see also http://webbook.nist.gov/chemistry and enter the formula for HCl. Check the box for Other Data—Constants of Diatomic Molecules. Scroll to the bottom of the table where the data for the ground state ($X\ ^1\Sigma^+$) are listed.
6. See P. Atkins and J. De Paula, *Physical Chemistry,* 8th ed., pp. 320–328, W. H. Freeman (New York), 2002.

Further Readings

J. B. Foresman and Æ Frisch, *Exploring Chemistry with Electronic Structure Methods: A Guide to Using Gaussian*, 1st ed., pp. 112–113, 141, Gaussian, Inc. (Pittsburgh PA), 1993.

I. N. Levine, *Quantum Chemistry*, 5th ed., pp. 492–493, 563–568, Prentice Hall (Upper Saddle River, NJ), 2000.

Appendix

The CCSD(T)/aug-cc/pVDZ values obtained from a scan from Step 1 as it appears in the archive (very bottom) of the Gaussian output file:

CCSD(T) = −460.1820317,−460.2407796,−460.2663741,−460.2722674,−460.2667144, −460.2548048,−460.2397061,−460.2234106,−460.2071777

Introduction to Gaussian

Gaussian is a program that allows for efficient electronic structure calculations. GaussView is the graphical user interface

Electronic structure methods allow for the computation of molecular properties. The energy and properties can be determined by solving the Schrödinger equation. Exact methods are difficult to obtain and there are several different methods that can be used for calculation.

1. Semi-empirical methods-This class of electronic structure methods uses parameters derived from experimental data to simplify the calculation. This is efficient however as they rely on parameters this method may not yield accurate results if the chemical system deviates from the systems used for parameters.
2. Ab initio methods-utilize quantum mechanics and mathematical approximations
3. Density Functional Theory- Similar to ab initio methods, however electron correlation effects (the fact that one electron is influenced, and influences the other electrons) are taken into account.

There are different functional forms and approximations within these methods. In addition to the functional a basis set is also necessary. A basis set is a mathematical description of the orbitals. The complexity of the basis set varies from basis set types. Larger basis sets improve the accuracy of the calculation but increases the computational expenditure. With most computations the question of cost vs accuracy must be addressed

The setup of the input file is fairly simple:

1. Specify the checkpoint file
2. Route section. This is where the functional and the basis set are specified as well as any commands for the calculation
3. Space
4. Title section-This is for the user to document what they are calculating
5. Space
6. Charge and multiplicity
    a. Charge is the integer value of the charge on the whole system under analysis
    b. Spin of the system. This can be calculated by 2S+1; S is the total spin. Paired electrons don't contribute to spin as their opposing spin values cancel each other out. Each unpaired electron adds +1/2 to S.
7. Molecular structure information: This is the starting geometry for the calculation. It can be specified by creating a Z-matrix, giving a guess geometry, or taking coordinates that have been experimentally determined (from the protein database, etc)

Basic Input File:

```
%chk=h2so4_3_wat_1_opt.chk
# mp2/aug-cc-pVTZ opt

h2so4 n=3 water conf 1

0 1
S       0.44894     -0.62250     -0.33816
O      -0.01128     -0.95630      1.11848
O       0.38994      0.97701     -0.37566
H       1.22408      1.31311      0.06039
H      -1.01059     -0.76788      1.19785
O       1.83055     -1.03293     -0.43604
O      -0.53795     -1.05997     -1.28806
O      -2.49577     -0.34288      1.29193
H      -2.59771      0.38364      0.63690
H      -3.09787     -1.03918      1.00850
O       2.78423      1.42169      0.62400
H       2.99815      0.49837      0.41913
H       2.94968      1.51756      1.56729
O      -2.40341      1.62528     -0.60316
H      -1.43508      1.67009     -0.65078
H      -2.66410      1.32892     -1.48069
```

This particular input file was uses the MP2 level of theory with the aug-cc-pVTZ basis set. The calculation was preformed on one of LSU's supercomputers and shouldn't be calculated on a local computer at this level of theory. This calculation involves sulfuric acid and three water molecules and was part of a series of calculations to determine when sulfuric acid would experience its first deprotonation. Electronic structure calculations are totally determined by the electronic structure and therefore the bonds aren't specified and can break and form.

Another way to set up a calculation is to directly open Gaussian09 click file->new and then add the specific information like the following:

Exercise 1: follow the example and optimize HCl

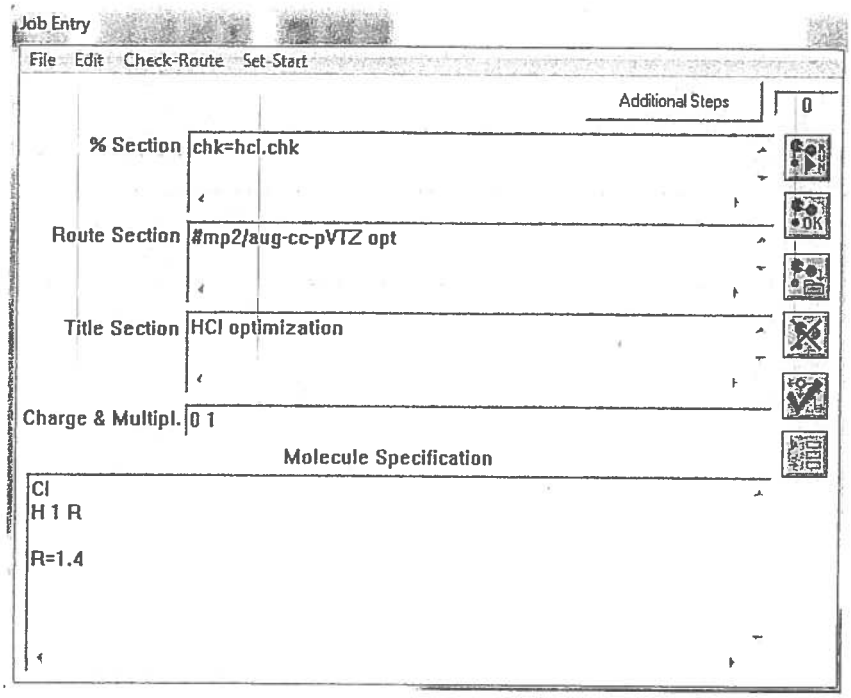

This format has all the required information as the previous calculation. This one is simply optimizing the HCl. The difference in this calculation is that the Molecular Specification was not given as Cartesian coordinates, but rather internal coordinates, where the H is placed R distance away from atom 1, which in this case is Cl. The given distance was 1.4 Angstroms, and when optimized:

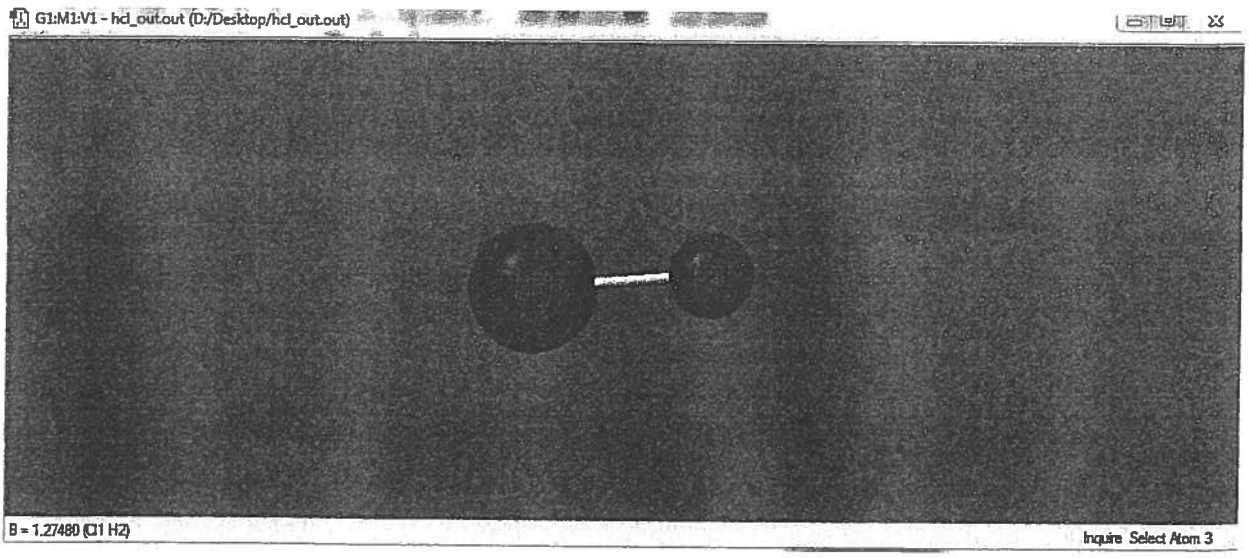

The HCl distance was found to be about 1.27 angstroms. Had the keyword opt not been included in the input section, the calculation would have done a single point calculation (it would just calculate the energy at the given coordinates). Try this and compare the energies.

The optimization keyword allows for the program to "search" for a minimum energy structure. This is done using the gradient of energy until convergence is reached. This may find a saddle point, local minima, or global minima, which is why it is essential to start with a 'good' starting structure. The structure of your minima is dependent on the starting structure.

Frequencies: Adding the term freq to the route section will allow for the calculation of frequencies. These are useful for calculation of force constants, prediction of IR spectra, identification of stationary points, and for corrections to calculated thermodynamic properties. They are calculated from the second derivative of energy with respect to nuclear positions.

Here is an input file for you to try:

Exercise 2: examine molecular orbitals as well as vibrational frequencies

```
%chk=co2z.chk
#p ub3lyp/lanl2dz pop=(full,npa) opt freq

Molecular orbital calculation and vibrational frequencies of co2

0 1
C
O   1 R1
O   1 R1 2 180.0
Variables:
R1 1.1612
```

This particular calculation optimizes the geometry, calculates the frequencies, and the addition of pop=(full,npa) prints the full molecular orbital data from the natural population analysis.

Once the calculation is completed, the checkpoint file can be opened in Gaussview. To view the molecular orbitals you can go to edit-> MO -> Visualize, click a molecular orbital to highlight and click update.

To view the frequencies open the output file in Gaussview. Click Results-> Vibrations. You can click on any of the modes and then start animation to view the movement. The intensities are also given in the table. (See next page) The predicted spectrum can be visualized by clicking spectrum, however it is important to keep in mind that while the frequency and intensity of the lines were calculated, the width is given arbitrarily.

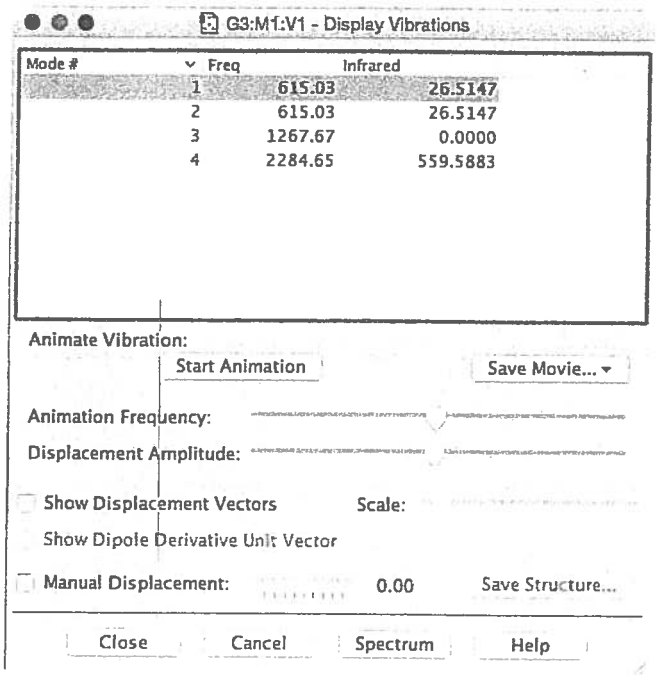

A summary of the results from a calculation can be taken from going to Results->Summary. For the carbon dioxide the output would look like this:

G3:M1:V1 - Gaussian Calculation Summary

Molecular orbital calculation and vibrational frequencies co2		
File Name	co2z	
File Type	.log	
Calculation Type	FREQ	
Calculation Method	UB3LYP	
Basis Set	LANL2DZ	
Charge	0	
Spin	Singlet	
E(UB3LYP)	-188.54011918	a.u.
RMS Gradient Norm	0.00000661	a.u.
Imaginary Freq	0	
Dipole Moment	0.0000	Debye
Point Group	D*H	
Job cpu time:	0 days 0 hours 0 minutes 2.4 seconds.	

Ok View File Save Data

Keep in mind that the energy is given in atomic units

Exercise 3:

Calculate the energy and frequency of HCl using the ccsd(t) and the aug-cc-pvtz basis set with these coordinates:

H	0.00000000	0.00000000	0.00000000
Cl	0.00000000	0.00000000	1.27000000

Exercise 4:

Use the same coordinates as above but change the y coordinate of the Cl to 1. Attempt a potential energy scan across the hcl distance. Hint: the keyword opt=ModRed requests a relaxed potential energy scan. Also after the coordinate specification you will have to include a line saying what you want scanned.

Element_scanned Element_number Element_number S number_of_scans interval_of_scan

After you receive your assignment: prepare input file .gjf as described in your textbook/website.

Example assignments;

1) calculate HCl (or DCl or HBr or DBr frequencies and show results with animation), suggested methods HF or RHF → and IR spectrum
2) calculate TD functions of benzene or naphthalene at 300K 1atm
3) calculate vibrations of benzene or naphthalene
4) calculate electronic potential of HCl for 10 points using SCAN function (go directly to Gaussian , not Gauss View) using model and base set `ccsd(t)/aug-cc-pvtz`
5) calculate energy and molecular orbitals and show molecular orbitals for naphthalene using `b3lyp/6-31+G(d)`
6) calculate NMR spectrum of benzene (advanced)

Geometries:

Benzene

```
6           0.000000    1.396619    0.000000
6           1.209508    0.698310    0.000000
6          -1.209508    0.698310    0.000000
6           1.209508   -0.698310    0.000000
6          -1.209508   -0.698310    0.000000
6           0.000000   -1.396619    0.000000
1           0.000000    2.483617    0.000000
1           2.150875    1.241808    0.000000
1          -2.150875    1.241808    0.000000
1           2.150875   -1.241808    0.000000
1          -2.150875   -1.241808    0.000000
1           0.000000   -2.483617    0.000000
```

benzoic acid

```
C 0.03626666666666667 -1.3137333333333332 0.06193333333333333
C 1.4352666666666667 -1.3137333333333332 0.06193333333333333
C 2.135266666666667 -0.10273333333333312 0.06193333333333333
C 1.4352666666666667 1.1092666666666668 0.06193333333333333
C 0.03626666666666667 1.1092666666666668 0.06193333333333333
C -0.6637333333333333 -0.10273333333333312 0.06193333333333333
C -2.1037333333333335 -0.10173333333333323 0.06093333333333333
O -2.706733333333333 -1.1437333333333333 0.06093333333333333
O -2.7747333333333333 1.0632666666666666 0.05993333333333333
H -0.5067333333333334 -2.2587333333333333 0.06193333333333333
H 1.9802666666666666 -2.2577333333333334 0.06193333333333333
H 3.2252666666666667 -0.10273333333333312 0.06193333333333333
H 1.9802666666666666 2.0532666666666666 0.06193333333333333
H -0.5067333333333334 2.054266666666667 0.06193333333333333
H -3.001733333333333 1.3082666666666667 -0.8630666666666668
```

Napthalene

C -1.0261711352653762 1.374203209686488 -0.5724762702374843
C -2.2605244880810678 0.737570938945495 -0.6410650118144827
C -2.397864317378605 -0.6236532743077187 -0.33468717292887146
C -1.2845216995206103 -1.3739852352172743 0.05817393062993007
C -0.04064031556226016 -0.7293272126217363 0.16071895445869772
H -1.3956954963173658 -2.447223721399662 0.30045577193994755
H -3.378025733863516 -1.0944084394838827 -0.3845449466092944
H -3.1305240800257645 1.315049269793162 -0.9343418685697398
H -0.935591941088477 2.434266131287722 -0.8200310552539497
C 1.0844368257552817 -1.4298759558300005 0.5904436310439122
C 2.3224206605546884 -0.7927429985296366 0.7001161606331444
C 2.481835535127136 0.5580591907495254 0.3807483362065216
C 1.3972333007299906 1.310359573719593 -0.05133804279514124
H 1.5340734984683766 2.352497935280988 -0.34885275917585595
H 3.461389699958172 1.024140549129248 0.45881731037908374
H 3.179459912149262 -1.3649533267386011 1.0376579524572767
H 1.0079655821115816 -2.4843680472025444 0.8518906501888984
C 0.08503002370576217 0.6459054468740536 -0.15968575272776847

HCl (potential surface /curve scan0

H
Cl 1 r

r 1.0 8 .1

HCl

H 0. 0. 0.
Cl 0. 0. 1.27

DCl

H 0. 0. 0.
Cl 0. 0. 1.27

CO2

C 0.0 0.0 0.0
O1 0.0 0.0 1.161204
O2 0.0 0.0 -1.161204

Models/basis set:

b3lyp/6-31+G(d)

RHF/6-31G(d)

HF STO-3G

ccsd(t)/aug-cc-pvtz

Work: SCAN Opt Freq=ReadIso POP=(FULL,NPA)			

```
%NProcl=4
%mem=2000000,7000000
%chk=hcl.chk
#p ccsd(t)/aug-cc-pvdz scan

HCL D

0 1
H
Cl 1 r

r 1.0 8 .1
```

```
#Chk=Dcl.chk
#HF  STO-3G
# Opt Freq=ReadIso

hcl freq

  0 1
 H     0. 0. 0.
 Cl   0.   0.   1.27

 300 1. 0.91
2
35
```

```
%Chk=benzacid5.chk
#p b3lyp/6-31+G(d) scf(MaxCycle=300,tight)
# GFPrint POP=(FULL,NPA)

benzoic acid

0 1
C 0.03626666666666667 -1.3137333333333332 0.06193333333333333
C 1.4352666666666667 -1.3137333333333332 0.06193333333333333
C 2.135266666666667 -0.10273333333333312 0.06193333333333333
C 1.4352666666666667 1.1092666666666668 0.06193333333333333
C 0.03626666666666667 1.1092666666666668 0.06193333333333333
C -0.6637333333333333 -0.10273333333333312 0.06193333333333333
C -2.1037333333333335 -0.10173333333333323 0.06093333333333333
O -2.706733333333333 -1.1437333333333333 0.06093333333333333
O -2.7747333333333333 1.0632666666666666 0.05993333333333333
H -0.5067333333333334 -2.2587333333333333 0.06193333333333333
H 1.9802666666666666 -2.2577333333333334 0.06193333333333333
H 3.2252666666666667 -0.10273333333333312 0.06193333333333333
H 1.9802666666666666 2.0532666666666666 0.06193333333333333
H -0.5067333333333334 2.054266666666667 0.06193333333333333
H -3.001733333333333 1.3082666666666667 -0.8630666666666668
```

```
%chk=napth3.chk
#p b3lyp/6-31G(d) scf(MaxCycle=300,tight)
# GFPrint POP=(FULL,NPA)
# Opt Freq

DNapthalene  this try on runG03 ... 4 MP5L

0 1
C -1.0261711352653762 1.374203209686488 -0.5724762702374843
C -2.2605244880810678 0.737570938945495 -0.6410650118144827
C -2.397864317378605 -0.6236532743077187 -0.33468717292887146
C -1.2845216995206103 -1.3739852352172743 0.05817393062993007
C -0.04064031556226016 -0.7293272126217363 0.16071895445869772
H -1.3956954963173658 -2.447223721399662 0.30045577193994755
H -3.378025733863516 -1.0944084394838827 -0.3845449466092944
H -3.1305240800257645 1.315049269793162 -0.9343418685697398
H -0.935591941088477 2.434266131287722 -0.8200310552539497
C 1.0844368257552817 -1.4298759558300005 0.5904436310439122
C 2.3224206605546884 -0.7927429985296366 0.7001161606331444
C 2.481835535127136 0.5580591907495254 0.3807483362065216
C 1.3972333007299906 1.310359573719593 -0.05133804279514124
H 1.5340734984683766 2.352497935280988 -0.34885275917585595
H 3.461389699958172 1.024140549129248 0.45881731037908374
H 3.179459912149262 -1.3649533267386011 1.0376579524572767
H 1.0079655821115816 -2.4843680472025444 0.8518906501888984
C 0.08503002370576217 0.6459054468740536 -0.15968575272776847

300 1.0 0.9135
12
12
12
12
12
1
1
1
1
12
12
12
12
1
1
1
1
12
```

```
%chk=C:\Users\chrupn\Desktop\co2zxx.chk
#p freq ub3lyp/lanl2dz pop=(npa,full) geom=connectivity #guess=(mix,print)

charge = 0       spin =0 (multiplicity 1)

0 1
 C                  0.00000000    0.00000000    0.00000000
 O                  0.00000000    0.00000000    1.16120000
 O                  0.00000000    0.00000000   -1.16120000

 1 2 2.0 3 2.0
 2
 3

 300 1.0 0.9135
 6
 8
 8
```

```
%Chk=benzacid2.chk
#p RHF/6-31(d)    Opt Freq=ReadIso

benzoic acid

0 1
C 0.03626666666666667 -1.3137333333333332 0.06193333333333333
C 1.4352666666666667 -1.3137333333333332 0.06193333333333333
C 2.135266666666667 -0.10273333333333312 0.06193333333333333
C 1.4352666666666667 1.1092666666666668 0.06193333333333333
C 0.03626666666666667 1.1092666666666668 0.06193333333333333
C -0.6637333333333333 -0.10273333333333312 0.06193333333333333
C -2.1037333333333335 -0.10173333333333323 0.06093333333333333
O -2.706733333333333 -1.1437333333333333 0.06093333333333333
O -2.7747333333333333 1.0632666666666666 0.05993333333333333
H -0.5067333333333334 -2.2587333333333333 0.06193333333333333
H 1.9802666666666666 -2.2577333333333334 0.06193333333333333
H 3.2252666666666667 -0.10273333333333312 0.06193333333333333
H 1.9802666666666666 2.0532666666666666 0.06193333333333333
H -0.5067333333333334 2.054266666666667 0.06193333333333333
H -3.001733333333333 1.3082666666666667 -0.8630666666666668

300 1.0 0.9135
12
12
12
12
12
12
12
16
16
1
1
1
1
1
1
```

```
%chk=hclt.chk
#p ccsd(t)/aug-cc-pvtz scan

HCL D

0 1
H
Cl 1 r

r 1.0 8 .1
```

Models/basis set:

b3lyp/6-31+G(d)

RHF/6-31G(d)

HF STO-3G

ccsd(t)/aug-cc-pvtz

Work: SCAN Opt Freq=ReadIso POP=(FULL,NPA)		

FIGURE 1
An Excel spreadsheet comparing potential energy curves calculated for HCl for Morse and harmonic oscillator models with ab initio quantum mechanical results obtained with the program Gaussian. The example illustrates the use of cell formulas and some of the text Format options, such as bold and italic fonts of various sizes, subscripts and superscripts, and Greek and other special characters.

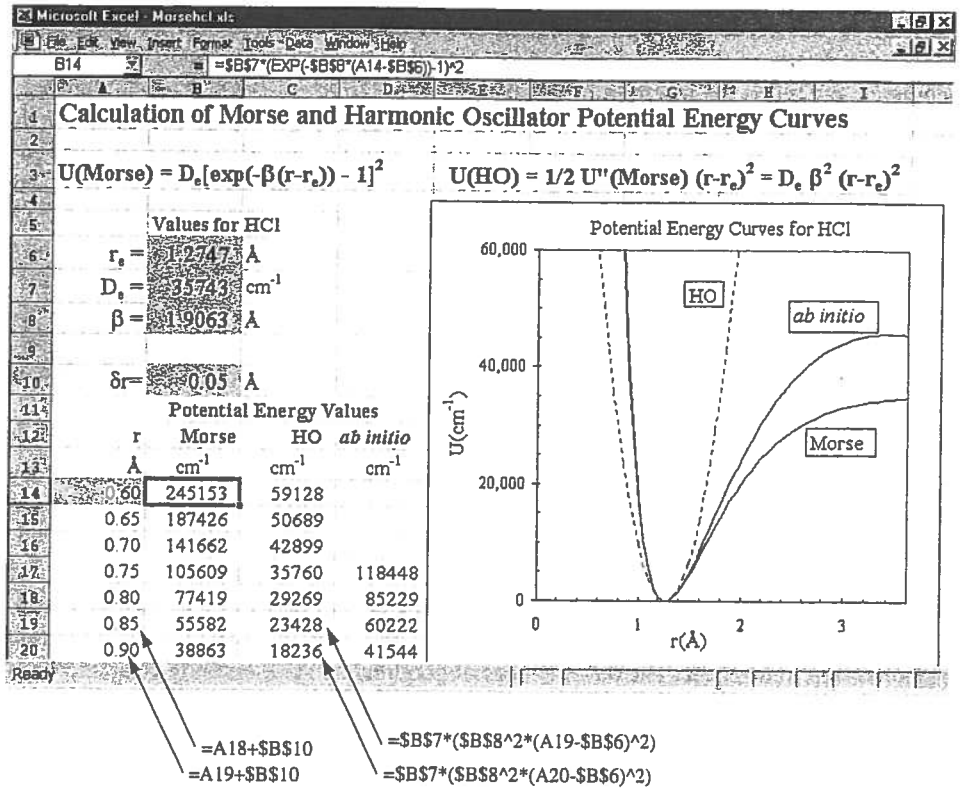

size, color, outlining, and so on. The Open and Save operations in the File menu can be used to open or save a spreadsheet, and the Print operation in this menu allows one to print all or a portion of the worksheets, including graphs, as in Fig. 1. You should experiment freely in order to become comfortable with these various manipulations.

DATA ENTRY AND MANIPULATION

Text and numerical data are entered into a cell by simply moving to the desired location and typing it. In the Excel worksheet example of Fig. 1, potential energy curves are calculated for Morse and harmonic oscillator models of a diatomic molecule from parameters entered into cells B6, B7, and B8. Data from a calculation using the ab initio quantum mechanical program Gaussian, described later, have been entered into column D. Under an operating system such as Windows, this transfer is easily effected by Copying the desired data from one Windows program to an intermediate Clipboard and then Pasting it into the spreadsheet or, in some cases, by directly "dragging" a selected block between two active programs. Alternatively, data files in standard ASCII form can be directly read into a spreadsheet and parsed as desired to separate into columns *x*, *y*, and other text or numerical quantities.

Text can be displayed, and printed, in various fonts and font sizes, as subscripts or superscripts, or as special math or Greek characters by modifying the characteristics of cell entries under the Format options at the top of the worksheet (also accessible via the right mouse button). Similarly, one can choose centering or left–right adjustment (alignment) of the text or numbers, bold or italic text, the widths of columns, and the format of numerical entries (0.00560 or 5.60E2, $27.37, etc.). Numerical data typically are stored and generated with at least 15 digits of accuracy, regardless of the number entered or displayed. Other spreadsheet niceties include color choices for text and shading and outlining

A similar conclusion is reached if $U(r)$ is taken to have the Morse potential form given by Eq. (9) of Exp. 39. In both cases, the mass dependence of $\tilde{\nu}_e x_e$ is found to be greater than for $\tilde{\nu}_e$ and is

$$\frac{\tilde{\nu}_e^* x_e^*}{\tilde{\nu}_e x_e} = \frac{\mu}{\mu^*} \tag{15}$$

Equations (13) and (15) are useful in obtaining the $\tilde{\nu}_0^*$ counterpart of Eq. (8),

$$\tilde{\nu}_0^* = \tilde{\nu}_e^* - 2\tilde{\nu}_e^* x_e^* = \tilde{\nu}_e \left(\frac{\mu}{\mu^*}\right)^{1/2} - 2\tilde{\nu}_e x_e \frac{\mu}{\mu^*} \tag{16}$$

and it is seen that a measurement of $\tilde{\nu}_0$ for HCl and DCl suffices for a determination of $\tilde{\nu}_e$ and $\tilde{\nu}_e x_e$. Alternatively of course the latter constants can be determined from overtone vibrations ($\Delta v > 1$) of a single isotopic form (see Exp. 39). However, such overtones generally have low intensity and the transitions may fall outside the range of many infrared instruments, so the isotopic shift method is used in the present experiment.

Since HCl gas is a mixture of $H^{35}Cl$ and $H^{37}Cl$ molecules, a chlorine isotope effect will also be present. However, the ratio of the reduced masses is only 1.0015: therefore high resolution is required to detect this effect. HCl is predominantly $H^{35}Cl$, and for this experiment we shall assume that the HCl bands obtained are those of $H^{35}Cl$. If deuterium is substituted for hydrogen, the ratio of the reduced masses, $\mu(D^{35}Cl)/\mu(H^{35}Cl)$, is 1.946 and the isotope effect is quite large.

Vibrational Partition Function.[4,5] The thermodynamic quantities for an ideal gas can usually be expressed as a sum of translational, rotational, and vibrational contributions (see Exp. 3). We shall consider here the heat capacity at constant volume. At room temperature and above, the translational and rotational contributions to C_v are constants that are independent of temperature. For HCl and DCl (diatomic and thus linear molecules), the molar quantities are

$$\tilde{C}_v(\text{trans}) = \tfrac{3}{2}R$$

$$\tilde{C}_v(\text{rot}) = R \tag{17}$$

The vibrational contribution to $\tilde{C}_v$ varies with temperature and can be calculated from the vibrational partition function q_{vib} using

$$\tilde{C}_v(\text{vib}) = R\frac{\partial}{\partial T}\left(T^2 \frac{\partial \ln q_{\text{vib}}}{\partial T}\right) \tag{18}$$

The partition function q_{vib} of HCl or DCl is well approximated by the harmonic-oscillator partition function q^{HO}. Since the energy levels of a harmonic oscillator are given by $(v + \frac{1}{2})h\nu$, one obtains[4]

$$q^{\text{HO}} = \sum_{v=0}^{\infty} \exp\left[\frac{-(v+\frac{1}{2})h\nu}{kT}\right] = \frac{e^{-h\nu/2kT}}{1 - e^{-h\nu/kT}} \tag{19}$$

Combining Eqs. (18) and (19), we find

$$\tilde{C}_v(\text{vib}) = R\frac{u^2 e^{-u}}{(1-e^{-u})^2} \tag{20}$$

where $u = h\nu/kT = hc\tilde{\nu}/kT = 1.4388\tilde{\nu}/T$.

Intensities and Statistical Weights. The absolute absorption intensity of a vibrational–rotational transition is proportional to the square of the transition moment P_{ij} times the population in the lower state. P_{ij} varies only slightly for different rotational levels, so the principal factors determining the relative intensity are the degeneracy and the Boltzmann weight for the lower level,

$$I_J \propto g_I g_J \exp\left[\frac{-hcBJ(J+1)}{kT}\right] \tag{12}$$

The rotational degeneracy g_J is $2J + 1$, and the nuclear-spin degeneracy g_I varies with rotational level only when the molecule contains symmetrically equivalent nuclei.

A complete discussion of the factors that determine g_I is beyond the scope of this book but can be found in Refs. 5 and 7. Briefly, the total wavefunction Ψ_{tot} for molecules with equivalent nuclei must obey certain symmetry requirements upon exchange, as determined by the Pauli principle. Exchange of nuclei with half-integral spin, such as protons ($I = \frac{1}{2}$), must produce a sign change in Ψ_{tot}. Such nuclei are termed *fermions* and are distributed among energy levels according to Fermi–Dirac statistics. Nuclei with integral nuclear spin, such as deuterium ($I = 1$), obey Bose–Einstein statistics and are called *bosons;* for these the sign of Ψ_{tot} is unchanged by interchange of the equivalent particles. The total wavefunction can be written, approximately, as a product function,

$$\Psi_{tot} = \psi_{elec}\psi_{vib}\psi_{rot}\psi_{ns} \tag{13}$$

For the ground vibrational state of acetylene, $\psi_{elec}\psi_{vib}$ is symmetric with respect to nuclear exchange, so $\psi_{rot}\psi_{ns}$ must be antisymmetric for C_2H_2, symmetric for C_2D_2. For linear molecules the ψ_{rot} functions are spherical harmonics that are symmetric for even J, antisymmetric for odd J.[5,7] The ψ_{ns} spin-product functions for two protons consist of three that are symmetric ($\alpha\alpha$, $\alpha\beta + \beta\alpha$, $\beta\beta$) and one that is antisymmetric ($\alpha\beta - \beta\alpha$), where α and β are the functions corresponding to M_I values of $+\frac{1}{2}$ and $-\frac{1}{2}$ (see Exp. 32). Thus for C_2H_2, it follows that g_I is 1 for even J, 3 for odd J, and the P and R branch lines will alternate in intensity. For C_2D_2, with spin functions α, β, γ representing the M_I values of $+1, 0, -1$, there are six symmetric nuclear spin combinations ($\alpha\alpha$, $\beta\beta$, $\gamma\gamma$, $\alpha\beta + \beta\alpha$, $\alpha\gamma + \gamma\alpha$, $\beta\gamma + \gamma\beta$) and three that are antisymmetric to exchange ($\alpha\beta - \beta\alpha$, $\alpha\gamma - \gamma\alpha$, $\beta\gamma - \gamma\beta$). Consequently the *even* J rotational lines are stronger in this case. The experimental observation of such intensity alternations confirms the $D_{\infty h}$ symmetry of acetylene, and in the present experiment serves as a useful check on the assignment of the J values for the P and R branch transitions.

EXPERIMENTAL

An infrared grating or Fourier-transform (FTIR) spectrometer covering the spectral region from 600 to 4000 cm^{-1} is sufficient for this experiment, although extension to 400 cm^{-1} is desirable if the ν_5 band of C_2D_2 at about 540 cm^{-1} is to be studied. Table 2 indicates the spectral regions of interest and the approximate pressures that give satisfactory intensities. These pressures may require some adjustment depending on the resolution capabilities of the instrument, since the peak absorbance of a narrow line increases as the spectral resolution improves. For the survey scan, a resolution of 4 cm^{-1} is adequate to permit rapid data collection at reasonable signal-to-noise ratio. The regions to be studied in detail should be examined at an expanded scale to permit accurate frequency measurements. A resolution of at least 1.5 cm^{-1} is needed to resolve the rotational structure of the

energy, E_v is the vibrational energy, and E_r is the rotational energy. This electronic energy E_{el} refers to the minimum value of the potential curve for a given electronic state. The zero of energy is arbitrarily taken as the minimum in the potential curve for the lowest electronic state (ground state). It is convenient to divide E_{int} by the quantity hc, where c is expressed in units of cm s^{-1}, to get the so-called *term value*, $T_{int}(cm^{-1}) = E_{int}/hc = T_{el} + G + F$, where the vibrational and rotational term values E_v/hc and E_r/hc are given their conventional symbols G and F, respectively. The advantage of this change is that the frequency $\tilde{\nu}$ (expressed in cm^{-1}) for a transition between two electronic states can be simply expressed by

$$\tilde{\nu} = T'_{el} - T''_{el} + G(v') - G(v'') + F(J') - F(J'') \quad (1a)$$

$$\simeq \tilde{\nu}_{el} + G(v') - G(v'') \quad (1b)$$

where $\tilde{\nu}_{el} = T'_{el} - T''_{el} = T'_{el}$ since $T''_{el} = 0$ for the ground electronic state. $G(v)$ is the vibrational term value, which for an anharmonic oscillator is

$$G(v) = \tilde{\nu}_e (v + \tfrac{1}{2}) - \tilde{\nu}_e x_e (v + \tfrac{1}{2})^2 + \tilde{\nu}_e y_e (v + \tfrac{1}{2})^3 + \ldots \quad (2)$$

The rotational-term difference $F(v', J') - F(v'', J'')$ will be ignored, since the rotational structure is not resolved in this experiment. The cubic term in $G(v)$ is also small and can be neglected in obtaining the transition frequency

$$\tilde{\nu}(v', v'') = \tilde{\nu}_{el} + \tilde{\nu}'_e (v' + \tfrac{1}{2}) - \tilde{\nu}'_e x'_e (v' + \tfrac{1}{2})^2 - \tilde{\nu}''_e (v'' + \tfrac{1}{2}) + \tilde{\nu}''_e x''_e (v'' + \tfrac{1}{2})^2 \quad (3)$$

If the quantum numbers v' and v'' are known, the measured frequencies in an absorption or emission spectrum can then be used with a multiple linear least-squares technique (see Chapter XXI) to determine the parameters $\tilde{\nu}_{el}$, $\tilde{\nu}'_e$, $\tilde{\nu}'_e x'_e$, $\tilde{\nu}''_e$, and $\tilde{\nu}''_e x''_e$.

An alternative analysis procedure that is often used concentrates on the determination of $\tilde{\nu}_e$, $\tilde{\nu}_e x_e$ parameters within each electronic state. Differences between levels in the upper state are obtained from

$$\Delta\tilde{\nu}(v') \equiv \tilde{\nu}(v' + 1, v'') - \tilde{\nu}(v', v'') \simeq \tilde{\nu}'_e - 2\tilde{\nu}'_e x'_e (v' + 1) \quad (4)$$

A plot of $\Delta\tilde{\nu}(v')$ versus v', termed a Birge–Sponer plot, will thus have a slope of $-2\tilde{\nu}'_e x'_e$ and an intercept of $\tilde{\nu}'_e - 2\tilde{\nu}'_e x'_e$. The values of $\Delta\tilde{\nu}(v')$ for all v'' values are combined in this plot, so the two methods should give the same $\tilde{\nu}'_e$ and $\tilde{\nu}'_e x'_e$ parameters. A similar treatment can be used for lower-state differences $\Delta\tilde{\nu}(v'')$ to yield $\tilde{\nu}''_e$ and $\tilde{\nu}''_e x''_e$. The electronic spacing $\tilde{\nu}_{el}$ is then determined using these parameters and the observed frequencies in Eq. (3). This alternative procedure has the virtue of providing a visual representation of the data so that discordant points can be examined and the data can be fitted with a single least-squares treatment that is easily done on a personal computer. The multiple linear regression technique is preferred however, since it uses all the data with equal weighting and has minimum opportunity for calculational error in forming differences. Such regressions are easily performed with spreadsheet programs, as discussed in Chapter III.

Dissociation Energies. Because of the anharmonicity term, the spacing between adjacent vibrational levels decreases at higher v values, going to zero at the point of dissociation of the molecule into atoms. From Eq. (4), the value of $v = v_{max}$ at which this occurs is $v_{max} = (1/2x_e) - 1$. Substitution of this into Eq. (2) gives an expression for the energy D_e required to dissociate the molecule into atoms:

$$D_e = G(v_{max}) = \frac{\tilde{\nu}_e (1/x_e - x_e)}{4} \quad (5)$$

The energy D_0 to dissociate from the $v = 0$ level is smaller than D_e by the zero-point energy $G(0) = \tilde{\nu}_e/2 - \tilde{\nu}_e x_e/4$, so

$$D_0 = \frac{\tilde{\nu}_e(1/x_e - 2)}{4} \tag{6}$$

The expressions used in Eqs. (3) to (6) assume that $\tilde{\nu}_e y_e$ and higher-order anharmonicity terms can be neglected, an approximation that is good for the B state of I_2 but more typically leads to D_e values that are high by 10 to 30 percent. The error for the X ground electronic state is particularly large if only the absorption data are used to deduce $\tilde{\nu}_e''$, $\tilde{\nu}_e'' x_e''$, and D_e'', since only the $v'' = 0, 1, 2$ levels are appreciably populated at room temperature. Extension to higher levels, v'' up to ~30, is possible using the emission spectrum, so that improved values of $\tilde{\nu}_e''$ and $\tilde{\nu}_e'' x_e''$ are obtained. The value of D_e'' remains poorly determined however, since even the $v'' = 30$ level is less than halfway to the dissociation limit.

A more accurate value of D_e'' can be obtained by combining $\tilde{\nu}_{el}$ and D_e' values with $E(\mathrm{I}^*)$, the difference in electronic energy of the iodine atoms produced by dissociation from the X and B states. The value of $E(\mathrm{I}^*)$ is known to be 7603 cm^{-1} from atomic spectroscopy,[10] so that, as seen in Fig. 1,

$$D_e'' = \tilde{\nu}_{el} + D_e' - E(\mathrm{I}^*) \tag{7}$$

Potential Functions. Near the minimum in the potential-energy curve of a diatomic molecule, the harmonic-oscillator model is usually quite good. Therefore the force constant k_e can be calculated from the relation

$$k_e = \left(\frac{\partial^2 U}{\partial r^2}\right)_{r_e} = \mu(2\pi c \tilde{\nu}_e)^2 \tag{8}$$

where μ is the reduced mass and c is the speed of light in cm s^{-1} units. The constant k_e is the curvature of the potential curve at the minimum distance r_e and, like the dissociation energy, serves as a measure of the bond strength.

At large displacements from the equilibrium position, the harmonic representation of the potential energy is invalid and a more realistic model is necessary. One simple function that is often employed is the Morse potential,

$$U(r - r_e) = D_e\{\exp[-\beta(r - r_e)] - 1\}^2 \tag{9}$$

which has the desired values of 0 at $r = r_e$ and D_e at $r = \infty$. The parameter β is determined by equating k_e to the curvature of the Morse potential at $r = r_e$, yielding

$$\beta = \left(\frac{k_e}{2hcD_e}\right)^{1/2} \tag{10}$$

This three-parameter function provides a very good approximation to the real potential energy curve at all distances except $r \ll r_e$, a region of no practical significance.

Rotational Structure. Although rotational structure is not resolved in the present I_2 absorption experiment, each vibrational band consists of P ($\Delta J = -1$) and R ($\Delta J = +1$) branches as discussed in Exp. 37. For vibrational changes *within* a given electronic state, such as those measured for HCl in Exp. 37, the P and R branches are distinct, with a pronounced dip between them that characterizes the missing Q branch frequency for the "pure" vibrational transition (see Fig. 37-3). The spacing between lines in each branch is not constant, a slight asymmetry arising from a quadratic term [see Eqs. (37-9, 37-10; 38-11)]:

$$\tilde{\nu} = \tilde{\nu}_0 + (B' + B'')m + (B' - B'')m^2 \tag{11}$$

This is a general equation for the transition frequencies in which $m = -J$ for the P lines and $m = J + 1$ for the R lines. For $B' < B''$, the m^2 term causes a decrease (increase) in line spacing in the $R(P)$ branch at high J values. The resultant asymmetry is small for HCl, since $B' - B''$ is small.

If the upper and lower levels of a transition correspond to *different* electronic states, $B' - B''$ is generally much larger and the corresponding quadratic term in Eq. (11) will often cause a frequency maximum ($B' < B''$) in the R branch or a frequency minimum ($B' > B''$) in the P branch. This reversal in the progression of lines at low values of J produces a sharp *band head,* which in the case of I_2 occurs on the R branch edge at a J value as low as $J = 2$. The R branch thus folds back and merges with the P branch so that only a single band is seen for each transition to a vibrational level. A transition frequency measured at the intensity maximum of this band will be *lower* than the "pure" vibrational transition frequency $\tilde{\nu}_0$ assumed in Eq. (3). This error is not constant, varying from 20 to 50 cm^{-1} for I_2 as v' increases from 0 to the dissociation limit. In contrast the difference $\tilde{\nu}_{head} - \tilde{\nu}_0$ is quite small, varying from 0 to 0.13 cm^{-1}. For this reason, in the present experiment, band-head frequencies rather than band maxima will be measured to obtain the best values of the transition frequencies and the vibrational spacings.

The *emission* of bands of I_2 will also contain many rotational lines if the spectral width of the excitation source is broad enough to populate many upper-state levels. However, if the source is *monochromatic,* excitation to a single v', J' level can occur and the resultant spectral emission is greatly simplified. Assuming that there is no change to another level in the upper state owing to collisions, the emission to a given lower v'' level will consist of only the two transitions corresponding to $\Delta J = -1$ and $\Delta J = +1$. Since there is no restriction on Δv, one will observe sequences of doublets whose large spacings give the vibrational-level separations in the ground electronic state. The small spacing corresponds to $2B''(2J' + 1)$, the separation between the $J'' = J' + 1$ and $J'' = J' - 1$ levels in the lower v'' state. If a doublet of known J' value can be resolved, the splitting can be used to determine the rotational constant $B''(v'')$.

EXPERIMENTAL

Absorption Spectrum. The absorption spectrum of I_2 vapor is easily obtained with any commercial visible spectrometer having a resolution of about 0.2 nm or better; see Fig. 2. A general description of such spectrometers is given in Chapter XIX, and the instrument manual of the instrument to be used should be consulted for specific operational details. Follow the guidelines provided by the instructor in recording the spectra at the highest resolution possible with the instrument. Calibration corrections to the wavelength readout should be provided or made as described in Chapter XIX. Unless these are quite variable over the 450- to 650-nm range, a single correction value is sufficient.

Crystals of I_2 can be placed in a conventional glass cell of 100-mm length, which is then closed with a Teflon stopper. A usable spectrum can be obtained at room temperature (vapor pressure of I_2 ~0.2 Torr), although the absorption is much more intense if the cell is wrapped with heating tape to raise the temperature to ~40°C (vapor pressure ~1 Torr). In this case, to avoid condensation of I_2, the windows should be heated to a higher temperature by wrapping the ends of the cell with extra coils of heating tape.

Emission Spectrum. Several sources are suitable for exciting the emission spectrum of I_2. In previous editions of this text, the use of a low-pressure mercury discharge lamp was described, in which the green Hg line at 546.074 nm causes a transition from

APPENDIX C

Thermodynamic Quantities for Selected Substances at 298.15 K (25°C)

Substance	ΔH_f° (kJ/mol)	ΔG_f° (kJ/mol)	S° (J/mol-K)
Aluminum			
$Al(s)$	0	0	28.32
$AlCl_3(s)$	−705.6	−630.0	109.3
$Al_2O_3(s)$	−1669.8	−1576.5	51.00
Barium			
$Ba(s)$	0	0	63.2
$BaCO_3(s)$	−1216.3	−1137.6	112.1
$BaO(s)$	−553.5	−525.1	70.42
Beryllium			
$Be(s)$	0	0	9.44
$BeO(s)$	−608.4	−579.1	13.77
$Be(OH)_2(s)$	−905.8	−817.9	50.21
Bromine			
$Br(g)$	111.8	82.38	174.9
$Br^-(aq)$	−120.9	−102.8	80.71
$Br_2(g)$	30.71	3.14	245.3
$Br_2(l)$	0	0	152.3
$HBr(g)$	−36.23	−53.22	198.49
Calcium			
$Ca(g)$	179.3	145.5	154.8
$Ca(s)$	0	0	41.4
$CaCO_3$ (s, calcite)	−1207.1	−1128.76	92.88
$CaCl_2(s)$	−795.8	−748.1	104.6
$CaF_2(s)$	−1219.6	−1167.3	68.87
$CaO(s)$	−635.5	−604.17	39.75
$Ca(OH)_2(s)$	−986.2	−898.5	83.4
$CaSO_4(s)$	−1434.0	−1321.8	106.7
Carbon			
$C(g)$	718.4	672.9	158.0
$C(s$, diamond)	1.88	2.84	2.43
$C(s$, graphite)	0	0	5.69
$CCl_4(g)$	−106.7	−64.0	309.4
$CCl_4(l)$	−139.3	−68.6	214.4
$CF_4(g)$	−679.9	−635.1	262.3
$CH_4(g)$	−74.8	−50.8	186.3
$C_2H_2(g)$	226.77	209.2	200.8
$C_2H_4(g)$	52.30	68.11	219.4
$C_2H_6(g)$	−84.68	−32.89	229.5
$C_3H_8(g)$	−103.85	−23.47	269.9
$C_4H_{10}(g)$	−124.73	−15.71	310.0
$C_4H_{10}(l)$	−147.6	−15.0	231.0
$C_6H_6(g)$	82.9	129.7	269.2
$C_6H_6(l)$	49.0	124.5	172.8
$CH_3OH(g)$	−201.2	−161.9	237.6
$CH_3OH(l)$	−238.6	−166.23	126.8
$C_2H_5OH(g)$	−235.1	−168.5	282.7
$C_2H_5OH(l)$	−277.7	−174.76	160.7
$C_6H_{12}O_6(s)$	−1273.02	−910.4	212.1
$CO(g)$	−110.5	−137.2	197.9
$CO_2(g)$	−393.5	−394.4	213.6
$HC_2H_3O_2(l)$	−487.0	−392.4	159.8
Cesium			
$Cs(g)$	76.50	49.53	175.6
$Cs(l)$	2.09	0.03	92.07
$Cs(s)$	0	0	85.15
$CsCl(s)$	−442.8	−414.4	101.2
Chlorine			
$Cl(g)$	121.7	105.7	165.2
$Cl^-(aq)$	−167.2	−131.2	56.5
$Cl_2(g)$	0	0	222.96
$HCl(aq)$	−167.2	−131.2	56.5
$HCl(g)$	−92.30	−95.27	186.69
Chromium			
$Cr(g)$	397.5	352.6	174.2
$Cr(s)$	0	0	23.6
$Cr_2O_3(s)$	−1139.7	−1058.1	81.2
Cobalt			
$Co(g)$	439	393	179
$Co(s)$	0	0	28.4
Copper			
$Cu(g)$	338.4	298.6	166.3
$Cu(s)$	0	0	33.30
$CuCl_2(s)$	−205.9	−161.7	108.1
$CuO(s)$	−156.1	−128.3	42.59
$Cu_2O(s)$	−170.7	−147.9	92.36

Substance	ΔH_f° (kJ/mol)	ΔG_f° (kJ/mol)	S° (J/mol-K)
Fluorine			
$F(g)$	80.0	61.9	158.7
$F^-(aq)$	−332.6	−278.8	−13.8
$F_2(g)$	0	0	202.7
$HF(g)$	−268.61	−270.70	173.51
Hydrogen			
$H(g)$	217.94	203.26	114.60
$H^+(aq)$	0	0	0
$H^+(g)$	1536.2	1517.0	108.9
$H_2(g)$	0	0	130.58
Iodine			
$I(g)$	106.60	70.16	180.66
$I^-(aq)$	−55.19	−51.57	111.3
$I_2(g)$	62.25	19.37	260.57
$I_2(s)$	0	0	116.73
$HI(g)$	25.94	1.30	206.3
Iron			
$Fe(g)$	415.5	369.8	180.5
$Fe(s)$	0	0	27.15
$Fe^{2+}(aq)$	−87.86	−84.93	113.4
$Fe^{3+}(aq)$	−47.69	−10.54	293.3
$FeCl_2(s)$	−341.8	−302.3	117.9
$FeCl_3(s)$	−400	−334	142.3
$FeO(s)$	−271.9	−255.2	60.75
$Fe_2O_3(s)$	−822.16	−740.98	89.96
$Fe_3O_4(s)$	−1117.1	−1014.2	146.4
$FeS_2(s)$	−171.5	−160.1	52.92
Lead			
$Pb(s)$	0	0	68.85
$PbBr_2(s)$	−277.4	−260.7	161
$PbCO_3(s)$	−699.1	−625.5	131.0
$Pb(NO_3)_2(aq)$	−421.3	−246.9	303.3
$Pb(NO_3)_2(s)$	−451.9	—	—
$PbO(s)$	−217.3	−187.9	68.70
Lithium			
$Li(g)$	159.3	126.6	138.8
$Li(s)$	0	0	29.09
$Li^+(aq)$	−278.5	−273.4	12.2
$Li^+(g)$	685.7	648.5	133.0
$LiCl(s)$	−408.3	−384.0	59.30
Magnesium			
$Mg(g)$	147.1	112.5	148.6
$Mg(s)$	0	0	32.51
$MgCl_2(s)$	−641.6	−592.1	89.6
$MgO(s)$	−601.8	−569.6	26.8
$Mg(OH)_2(s)$	−924.7	−833.7	63.24
Manganese			
$Mn(g)$	280.7	238.5	173.6
$Mn(s)$	0	0	32.0
$MnO(s)$	−385.2	−362.9	59.7
$MnO_2(s)$	−519.6	−464.8	53.14
$MnO_4^-(aq)$	−541.4	−447.2	191.2
Mercury			
$Hg(g)$	60.83	31.76	174.89
$Hg(l)$	0	0	77.40
$HgCl_2(s)$	−230.1	−184.0	144.5
$Hg_2Cl_2(s)$	−264.9	−210.5	192.5
Nickel			
$Ni(g)$	429.7	384.5	182.1
$Ni(s)$	0	0	29.9
$NiCl_2(s)$	−305.3	−259.0	97.65
$NiO(s)$	−239.7	−211.7	37.99
Nitrogen			
$N(g)$	472.7	455.5	153.3
$N_2(g)$	0	0	191.50
$NH_3(aq)$	−80.29	−26.50	111.3
$NH_3(g)$	−46.19	−16.66	192.5
$NH_4^+(aq)$	−132.5	−79.31	113.4
$N_2H_4(g)$	95.40	159.4	238.5
$NH_4CN(s)$	0.0	—	—
$NH_4Cl(s)$	−314.4	−203.0	94.6
$NH_4NO_3(s)$	−365.6	−184.0	151
$NO(g)$	90.37	86.71	210.62
$NO_2(g)$	33.84	51.84	240.45
$N_2O(g)$	81.6	103.59	220.0
$N_2O_4(g)$	9.66	98.28	304.3
$NOCl(g)$	52.6	66.3	264
$HNO_3(aq)$	−206.6	−110.5	146
$HNO_3(g)$	−134.3	−73.94	266.4
Oxygen			
$O(g)$	247.5	230.1	161.0
$O_2(g)$	0	0	205.0
$O_3(g)$	142.3	163.4	237.6
$OH^-(aq)$	−230.0	−157.3	−10.7
$H_2O(g)$	−241.82	−228.57	188.83
$H_2O(l)$	−285.83	−237.13	69.91
$H_2O_2(g)$	−136.10	−105.48	232.9
$H_2O_2(l)$	−187.8	−120.4	109.6
Phosphorus			
$P(g)$	316.4	280.0	163.2
$P_2(g)$	144.3	103.7	218.1
$P_4(g)$	58.9	24.4	280
$P_4(s, \text{red})$	−17.46	−12.03	22.85
$P_4(s, \text{white})$	0	0	41.08
$PCl_3(g)$	−288.07	−269.6	311.7
$PCl_3(l)$	−319.6	−272.4	217
$PF_5(g)$	−1594.4	−1520.7	300.8
$PH_3(g)$	5.4	13.4	210.2
$P_4O_6(s)$	−1640.1	—	—
$P_4O_{10}(s)$	−2940.1	−2675.2	228.9
$POCl_3(g)$	−542.2	−502.5	325
$POCl_3(l)$	−597.0	−520.9	222
$H_3PO_4(aq)$	−1288.3	−1142.6	158.2

Substance	ΔH_f° (kJ/mol)	ΔG_f° (kJ/mol)	S° (J/mol-K)
Potassium			
$K(g)$	89.99	61.17	160.2
$K(s)$	0	0	64.67
$KCl(s)$	−435.9	−408.3	82.7
$KClO_3(s)$	−391.2	−289.9	143.0
$KClO_3(aq)$	−349.5	−284.9	265.7
$K_2CO_3(s)$	−1150.18	−1064.58	155.44
$KNO_3(s)$	−492.70	−393.13	132.9
$K_2O(s)$	−363.2	−322.1	94.14
$KO_2(s)$	−284.5	−240.6	122.5
$K_2O_2(s)$	−495.8	−429.8	113.0
$KOH(s)$	−424.7	−378.9	78.91
$KOH(aq)$	−482.4	−440.5	91.6
Rubidium			
$Rb(g)$	85.8	55.8	170.0
$Rb(s)$	0	0	76.78
$RbCl(s)$	−430.5	−412.0	92
$RbClO_3(s)$	−392.4	−292.0	152
Scandium			
$Sc(g)$	377.8	336.1	174.7
$Sc(s)$	0	0	34.6
Selenium			
$H_2Se(g)$	29.7	15.9	219.0
Silicon			
$Si(g)$	368.2	323.9	167.8
$Si(s)$	0	0	18.7
$SiC(s)$	−73.22	−70.85	16.61
$SiCl_4(l)$	−640.1	−572.8	239.3
$SiO_2(s,$ quartz)	−910.9	−856.5	41.84
Silver			
$Ag(s)$	0	0	42.55
$Ag^+(aq)$	105.90	77.11	73.93
$AgCl(s)$	−127.0	−109.70	96.11
$Ag_2O(s)$	−31.05	−11.20	121.3
$AgNO_3(s)$	−124.4	−33.41	140.9
Sodium			
$Na(g)$	107.7	77.3	153.7
$Na(s)$	0	0	51.45
$Na^+(aq)$	−240.1	−261.9	59.0
$Na^+(g)$	609.3	574.3	148.0
$NaBr(aq)$	−360.6	−364.7	141.00
$NaBr(s)$	−361.4	−349.3	86.82
$Na_2CO_3(s)$	−1130.9	−1047.7	136.0
$NaCl(aq)$	−407.1	−393.0	115.5
$NaCl(g)$	−181.4	−201.3	229.8
$NaCl(s)$	−410.9	−384.0	72.33
$NaHCO_3(s)$	−947.7	−851.8	102.1
$NaNO_3(aq)$	−446.2	−372.4	207
$NaNO_3(s)$	−467.9	−367.0	116.5
$NaOH(aq)$	−469.6	−419.2	49.8
$NaOH(s)$	−425.6	−379.5	64.46
Strontium			
$SrO(s)$	−592.0	−561.9	54.9
$Sr(g)$	164.4	110.0	164.6
Sulfur			
$S(s,$ rhombic)	0	0	31.88
$S_8(g)$	102.3	49.7	430.9
$SO_2(g)$	−296.9	−300.4	248.5
$SO_3(g)$	−395.2	−370.4	256.2
$SO_4^{2-}(aq)$	−909.3	−744.5	20.1
$SOCl_2(l)$	−245.6	—	—
$H_2S(g)$	−20.17	−33.01	205.6
$H_2SO_4(aq)$	−909.3	−744.5	20.1
$H_2SO_4(l)$	−814.0	−689.9	156.1
Titanium			
$Ti(g)$	468	422	180.3
$Ti(s)$	0	0	30.76
$TiCl_4(g)$	−763.2	−726.8	354.9
$TiCl_4(l)$	−804.2	−728.1	221.9
$TiO_2(s)$	−944.7	−889.4	50.29
Vanadium			
$V(g)$	514.2	453.1	182.2
$V(s)$	0	0	28.9
Zinc			
$Zn(g)$	130.7	95.2	160.9
$Zn(s)$	0	0	41.63
$ZnCl_2(s)$	−415.1	−369.4	111.5
$ZnO(s)$	−348.0	−318.2	43.9